NASA TECHNICAL NOTE

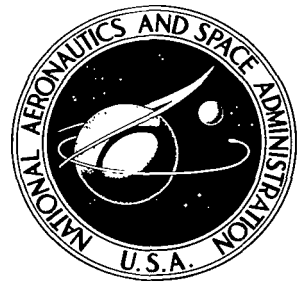

NASA TN D-8076

A COMPARISON OF MEASURED AND PREDICTED SPHERE SHOCK SHAPES IN HYPERSONIC FLOWS WITH DENSITY RATIOS FROM 4 TO 19

Charles G. Miller III

Langley Research Center
Hampton, Va. 23665

NATIONAL AERONAUTICS AND SPACE ADMINISTRATION • WASHINGTON, D. C. • DECEMBER 1975

1 Report No
NASA TN D-8076

2. Government Accession No.

3. Recipient's Catalog No.

4. Title and Subtitle

A COMPARISON OF MEASURED AND PREDICTED SPHERE SHOCK SHAPES IN HYPERSONIC FLOWS WITH DENSITY RATIOS FROM 4 TO 19

5. Report Date
December 1975

6. Performing Organization Code

7. Author(s)
Charles G. Miller III

8. Performing Organization Report No.
L-10445

10. Work Unit No.
506-26-20-01

11 Contract or Grant No.

13. Type of Report and Period Covered
Technical Note

14 Sponsoring Agency Code

9. Performing Organization Name and Address
NASA Langley Research Center
Hampton, Va. 23665

12 Sponsoring Agency Name and Address
National Aeronautics and Space Administration
Washington, D.C. 20546

15. Supplementary Notes

16 Abstract

This report presents measured shock shapes for sphere and hemisphere models in helium, air, CF_4, C_2F_6, and CO_2 test gases, corresponding to normal-shock density ratios (primary factor governing shock detachment distance of blunt bodies at hypersonic speeds) from 4 to 19. These shock shapes were obtained in three facilities at the Langley Research Center capable of generating the high density ratios experienced during planetary entry at hypersonic conditions; namely, the Langley 6-inch expansion tube, the Langley hypersonic CF_4 tunnel, and Langley pilot CF_4 Mach 6 tunnel (with CF_4 replaced by C_2F_6). Measured results are compared with several inviscid perfect-gas shock shape predictions, in which an effective ratio of specific heats is used as input, and with real-gas predictions which include effects of a laminar viscous layer and thermochemical nonequilibrium.

17. Key Words (Suggested by Author(s))
Hypersonic
Shock shapes
Real gas

18. Distribution Statement
Unclassified – Unlimited

Subject Category 34

19. Security Classif. (of this report)	20. Security Classif. (of this page)	21. No. of Pages	22. Price*
Unclassified	Unclassified	41	$3.75

*For sale by the National Technical Information Service, Springfield, Virginia 22161

A COMPARISON OF MEASURED AND PREDICTED SPHERE SHOCK SHAPES IN HYPERSONIC FLOWS WITH DENSITY RATIOS FROM 4 TO 19

Charles G. Miller III
Langley Research Center

SUMMARY

This report presents measured shock shapes for sphere and hemisphere models in helium, air, CF_4, C_2F_6, and CO_2 test gases, corresponding to normal-shock density ratios (primary factor governing shock detachment distance of blunt bodies at hypersonic speeds) from 4 to 19. These shock shapes were obtained in three facilities at the Langley Research Center capable of generating the high density ratios experienced during planetary entry at hypersonic conditions; namely, the Langley 6-inch expansion tube, the Langley hypersonic CF_4 tunnel, and Langley pilot CF_4 Mach 6 tunnel (with CF_4 replaced by C_2F_6). Measured results are compared with several inviscid perfect-gas shock shape predictions, in which an effective ratio of specific heats is used as input, and with real-gas predictions which include effects of a laminar viscous layer and thermochemical nonequilibrium.

INTRODUCTION

The practical importance of an accurate determination of shock detachment distance for proposed Earth and planetary entry vehicles is well established. Also, the role of shock detachment distance as a basis for comparison of theoretical methods for determining flow conditions about blunt bodies at supersonic and hypersonic speeds is recognized. (For some inverse methods, an accurate shock shape is required as input to enable the program to converge to a solution of the flow field.) Because the shock detachment distance and inviscid forebody flow for blunt bodies depend primarily on normal-shock density ratio and body geometry, the effect of real-gas phenomena (excitation of vibration, dissociation, and ionization energy modes) may have a significant effect on aerothermodynamic characteristics. Shock detachment distance results demonstrating these real-gas effects are primarily analytical.

The scarcity of experimental data at hypersonic-hypervelocity (high enthalpy) flow conditions motivated the study of reference 1. In reference 1, shock detachment distances for sphere, spherically blunted cone, and flat-faced cylinder models were measured in helium, air, and CO_2 test gases in the Langley 6-inch expansion tube. The free-stream velocities generated with these gases provided a range of normal-shock density ratio of 4 to 19. This highest value of density ratio is close to the value expected during peak heating for Martian

entry and is believed to be the highest value generated in a ground-based facility for which shock shapes were obtained about a stationary model at hypersonic conditions.

The importance of the shock shape measurements is enhanced by the fact that these measurements supplied information relating to the calibration of the expansion tube. As discussed in reference 1, shock shapes may provide information on the thermochemical state of the free-stream flow, on the flow within the shock layer about the test model, and on the uniformity of the free-stream flow. Of the models tested in reference 1, the shock detachment distance for the sphere is most sensitive to the effects of chemistry and flow nonuniformity. Now, the difference between measured (ref. 1) and predicted (refs. 2 and 3) shock shape for a sphere was observed to increase with increasing distance from the stagnation region. As noted in references 4, 5, and 6, this trend is indicative of free-stream flow-nonuniformity effects. A similar comparison of shock shape for flat-faced cylinder models revealed good agreement between measurement and prediction.

Primarily because of the conclusion that flow nonuniformity may exist in the expansion tube, a more comprehensive examination of the sphere data was undertaken. The experimental results for a sphere were compared with only two theoretical predictions in reference 1. Basic inputs to these two perfect-gas programs were effective values of Mach number and ratio of specific heats, which corresponded to the equilibrium real-gas value of normal-shock density ratio. Although these inputs provided good agreement between measured and predicted shock shapes for an extremely blunt body with sonic corners (flat-faced cylinder), they did not provide good agreement for a sphere. As noted in reference 1, significant discrepancies existed between the predictions of references 2 and 3 for the sphere in air and CO_2 flows. However, since reference 2 was the more rigorous computational scheme of the two and reference 3 was acknowledged to be an approximate technique, the predictions of reference 2 were weighed more heavily in the comparisons.

The purpose of this report is to present the results of a comprehensive comparison of measured shock shapes for a sphere with those of a number of prediction methods. This comparison represents a continuation of the analysis of sphere data of reference 1 and a reassessment of the conclusions drawn in this reference. As part of this comparison, shock shape results obtained in the Langley CF_4 tunnel (refs. 7 and 8) at a density ratio of 12 and Langley pilot CF_4 tunnel ($\text{with } CF_4 \text{ replaced by } C_2F_6$) at a density ratio of 15 for a hemisphere (ref. 9) are also compared with predicted values. These comparisons provide insight to the feasibility of using perfect-gas relations to predict real-gas phenomena, and illustrate agreement or lack of agreement between various theoretical methods with identical basic inputs. Although a number of studies have compared measured shock detachment distance with theory and theory with theory (for example, see reference listing in ref. 1), the present study represents the most extensive comparison for shock detachment distance on a sphere over a wide range of normal-shock density ratio.

SYMBOLS

d_n	sphere diameter, m
M	Mach number
N_{Re}	unit Reynolds number, per meter
p	pressure, N/m^2
r_n	sphere radius, m
T	temperature, K
U	velocity, m/sec
x,y	coordinates
γ	ratio of specific heats
γ_E	isentropic exponent
Δ	shock standoff distance on sphere axis of symmetry through stagnation point, m
δ	shock detachment distance normal to sphere surface
δ^*	boundary-layer displacement thickness measured normal to model surface, m
ϵ	normal-shock density ratio, ρ_2/ρ_1
θ	angle subtended by circular arc measured from sphere axis of symmetry through stagnation point, deg
λ	percent deviation of free-stream velocity at distance r_n from center-line value
ρ	density, kg/m^3

Subscripts:

0	free-stream stagnation conditions
1	free-stream static conditions

2	static conditions immediately behind normal portion of sphere bow shock
eff	effective (based on thermochemical equilibrium normal-shock density ratio considerations)
m	measured
pr	predicted
t	stagnation conditions behind normal bow shock

EXPERIMENTAL DATA

The experimental shock detachment distances for a sphere presented herein were obtained from three facilities at the Langley Research Center. These facilities, which possess the capability of generating the high normal-shock density ratios expected for Earth and planetary entries, are (1) the Langley 6-inch expansion tube, (2) the Langley hypersonic CF_4 tunnel, and (3) the Langley pilot CF_4 Mach 6 tunnel (with CF_4 replaced by C_2F_6). A brief description of these facilities, the corresponding test-flow conditions, and the models tested is presented.

Expansion Tube

The Langley 6-inch expansion tube is an impulse-type facility capable of generating hypersonic-hypervelocity (high-enthalpy) flows in arbitrary test gases. This facility, which is described in more detail in references 1 and 10, is basically a cylindrical tube divided by two diaphragms (primary and secondary) into three sections. For the present results, the driver or most upstream section was pressurized with helium to a nominal pressure of 33 MN/m^2. Two steel-primary-diaphragms separated this driver section from the adjoining section, denoted as the driven or intermediate section. After evacuation of this driven section, the helium, air, or CO_2 test gas was introduced to yield a quiescent pressure of 3.45 kN/m^2. The most downstream section, denoted as the acceleration section, was separated from the driven section by a thin, Mylar diaphragm (secondary diaphragm). The gas used as the test gas was also used as the acceleration gas for a given test, but at a lower quiescent pressure (3.1 N/m^2 for CO_2 to 22.0 N/m^2 for helium).

The operating sequence begins with the rupture of the steel diaphragms. A primary incident shock wave propagates into the quiescent test gas and encounters and ruptures the secondary diaphragm. A secondary incident shock wave propagates into the acceleration gas while an upstream expansion wave moves into the shock-heated test gas. In passing through this upstream expansion wave, the test gas undergoes an isentropic, unsteady expansion resulting

in an increase in flow velocity and free-stream Mach number. The theoretical gasdynamics of expansion tube flow is discussed in reference 11.

Shock shapes presented herein for helium, air, and CO_2 flows were obtained with a spherical model fabricated of stainless steel and having a radius r_n of 3.18 cm. (See ref. 1.) A single-pass schlieren system utilizing a vertical knife edge was employed, and shock shapes were recorded on negatives 10.7 cm by 12.7 cm. The point light source, which had a duration of approximately 150 nsec, was pulsed at a time 140 to 180 μsec into the 200 to 250 μsec quasi-steady test period. An electromagnetically collapsed aluminum foil shutter having an open-shut time of approximately 50 μsec was employed to reduce unwanted exposure during the postrun period.

Nominal flow conditions for each test gas are

Test gas	U_1, km/sec	M_1	$\gamma_{E,1}$	$N_{Re,1}$, per meter	ϵ	$\gamma_{E,2}$	$N_{Re,2}$, per meter
He	7.06	6.02	1.67	5.48×10^5	3.69	1.67	0.95×10^5
Air	5.32	7.72	1.32	7.95	11.11	1.15	2.60
CO_2	4.95	9.18	1.17	5.15	18.81	1.15	2.38

Langley Hypersonic CF_4 Tunnel

The Langley hypersonic CF_4 tunnel is a blowdown type facility having a maximum run time of 60 seconds. From a 33 MN/m^2 bottle field CF_4 is passed through stainless-steel tubes immersed in molten lead. This lead is heated by electric heaters immersed in the lead, and the piping between this lead-bath heater and the settling chamber is also heated with electric strip heaters. The heated CF_4 is expanded through an axisymmetric-contoured nozzle, which was designed for a Mach number of 6, and exhausts from the 50.8-cm-diameter nozzle exit into a 1.52-m-diameter tank. This tank is 1.83 m long with observation windows on opposite sides and on top. The vacuum system consists of three spheres having a total volume of 2266 m^3. Shock shape results presented herein for CF_4 were obtained on a 5.08-cm-radius hemisphere model by Raymond E. Midden of the Langley Research Center by using the shadowgraph technique.

Test flow conditions for the present CF_4 results are

$p_0 = 9.2$ MN/m^2 $\qquad$ $N_{Re,1} = 9.50 \times 10^5/m$

$T_0 = 702$ K $\qquad$ $\epsilon = 12.2$

$M_1 = 6.15$ $\qquad$ $\gamma_2 = 1.098$

$\gamma_1 = 1.203$ $\qquad$ $N_{Re,2} = 4.31 \times 10^5/m$

Langley Pilot CF_4 Mach 6 Tunnel (With CF_4 Replaced by C_2F_6)

Initial studies at the Langley Research Center to simulate real-gas effects at hypersonic conditions by using a test gas characterized by a low ratio of specific heats (specifically, CF_4) in a conventional-type wind tunnel are reported in references 7 and 8. The wind tunnel was a small pilot model equipped initially with a 5° half-angle conical nozzle having a 7.6-cm-diameter test section (ref. 7) and later with an axisymmetric-contoured nozzle terminating in a 15.24-cm-diameter test section. Exploratory tests conducted in this pilot model (with the contoured nozzle) to evaluate the feasibility of using C_2F_6 as the test gas are reported in reference 9.

The C_2F_6 pilot tunnel is an intermittent type supplied by two large bag-like accumulators which maintain a constant tunnel stagnation pressure for times as long as 3 minutes and eliminate contamination of the C_2F_6. The C_2F_6 passes from these accumulators through a lead-bath heat exchanger (stainless-steel tubes immersed in a bath of molten lead) into the stagnation chamber. The gas is then expanded through the contoured nozzle (designed for Mach 6 CF_4 flow) and exhausted into a 1200-m^3 vacuum sphere. To prevent the C_2F_6 gas from condensing during pumping from the storage bottles to the accumulators, the storage bottles and transport lines were wrapped with strip heaters and heated to 316 K. (C_2F_6 has a relatively high critical temperature of 292.7 K and relatively low critical pressure of 2.98 MN/m^2.)

Shock shapes presented herein for C_2F_6 were obtained from the shadowgraph film (original) illustrated in figure 16(c) of reference 9. This film illustrates the shock shape for a 1.27-cm-radius hemisphere. Test flow conditions corresponding to this particular shadowgraph film and read from the charts of reference 9 are

$p_0 = 15\ MN/m^2$	$N_{Re,1} = 1.19 \times 10^6/m$
$T_0 = 589\ K$	$\epsilon = 15.1$
$M_1 = 5.35$	$\gamma_2 = 1.060$
$\gamma_1 = 1.087$	$N_{Re,2} = 6.69 \times 10^5/m$

PREDICTION METHODS

A number of theoretical methods developed at the Ames Research Center and the Langley Research Center were used to predict the shock detachment distance for a sphere. A brief description of these methods is presented.

Barnwell's Method

The method of Barnwell is a two-step, time-dependent procedure of second-order accuracy for computing the inviscid, adiabatic flow at supersonic and hypersonic speeds about

plane and axisymmetric bodies with sharp corners and about smooth nonaxisymmetric bodies. This method is described in detail in reference 2 and a listing of the program and user's manual is given in reference 12.

A two-step finite-difference approximation to the time-dependent method of characteristics is used at the bow shock, whereas a two-step, time-dependent, finite-difference scheme is used at the surface of the body and between the shock and surface. The program may be exercised for a perfect gas or for thermochemical equilibrium air flow, and is formulated so that input γ may be given one value in the free stream and another value in the post-shock region. This capability with input γ was provided to approximate real-gas phenomena with a perfect gas model.

Steady flow results are obtained from this time-dependent method after many time steps when the difference in the solutions at consecutive time steps is sufficiently small (asymptotic solution to transient problem). It should be noted that both the method of reference 4 and of reference 2 were employed in reference 1 to examine the influence of a parabolic free-stream velocity distribution on the shock shape of a sphere. The predictions for uniform flow were generated by Richard W. Barnwell by using the method of reference 2, whereas he used the method of reference 4 to generate the nonuniform flow results. At the time of the study of reference 1, it was assumed that these two similar methods yielded the same shock detachment distance for a sphere over a range of flow conditions, for identical inputs to the perfect-gas mode of these programs. Results of a recent study show that this assumption is not correct. (See footnote on page 15.)

Method of Zoby and Graves

The method of reference 3 provides a rapid (in regard to computer time) means for predicting perfect gas, inviscid, supersonic and hypersonic flow conditions about spheres, ellipsoids, paraboloids, and hyperboloids which may have conical afterbodies. An approximation is made to the normal momentum equation which allows an independent evaluation of the pressure throughout the shock layer. This approximation removes many of the usual mathematical problems associated with subsonic and supersonic regions. An iterative technique which scales the shock to the specified body in the subsonic and low supersonic region of the flow field is used. In the downstream supersonic region of the flow field, the shock shape is computed by a marching procedure for successive points. Hence, the method is of an inverse nature in that a shock wave is assumed and calculations proceed along rays normal to the shock, but the shock shape is iterated until the specified body is obtained. A listing of the program and user instructions are presented in reference 3 along with a detailed discussion of the theory. Shock shapes presented herein and designated as being from reference 3 were generated by Ernest V. Zoby.

Method of Lomax and Inouye

The method of Lomax and Inouye (ref. 13) is an inverse finite-difference procedure (the shock-wave shape is assumed and the corresponding body computed) for the calculation of the inviscid flow field about an axisymmetric body traveling at hypersonic speeds. This method is confined to the subsonic region and the vicinity of this region. A solution is obtained that extends sufficiently far into the supersonic region to provide initial conditions for a continuing analysis by the method of characteristics. A one-parameter family of shock shapes was found to yield spherical-nosed axisymmetric bodies to a high degree of accuracy. Governing equations were placed in a shock-oriented coordinate system, where t is the axis of the shock itself and s is the axis of symmetry. Along with basic inputs for flow conditions and body geometry were inputs for increments of t and s and the shock-wave parameter A_5 of reference 13. (The value of A_5 was obtained from fig. 14(b) of ref. 13.) In some instances, a trial-and-error procedure on the inputs Δs and Δt was required to enable the program to run successfully. The method of reference 13 is applicable to thermochemical equilibrium gas flows as well as perfect gas flows. For the present study, the equilibrium gas mode was exercised for air and CO_2. Thermodynamic properties required for these calculations were obtained from tapes supplied to the Langley Research Center by the Ames Research Center.

Sutton's Method

A detailed description of the method of Sutton for the fully coupled solution of the radiative flow field about an ablating entry body is given in references 14 and 15. In this method, the flow field is separated into an outer layer where inviscid flow equations are applicable and an inner viscous layer where boundary-layer equations are applicable. Both laminar and turbulent boundary layers are considered. The inviscid flow field is solved for by using a second-order time-asymptotic procedure. In coupling the two layers, the inviscid flow field is displaced from the body surface by the boundary-layer displacement thickness. Boundary-layer profiles are used out from the surface to the point where the boundary-layer edge properties and their derivatives equal the corresponding inviscid layer values. Thermochemical equilibrium properties are determined for a given gas from the elemental mass fractions and two state properties (pressure and enthalpy).

Several program options are available. One is the fully coupled solution; a second is an inviscid flow-field solution; and the third is an inviscid stagnation-region solution. The second option was used by Kenneth Sutton to generate the shock shapes presented herein and designated as being from reference 14. During the course of this study, the program was modified by Kenneth Sutton to include the capability of using perfect-gas relations for obtaining the inviscid flow-field solution. Perfect-gas shock-shape predictions with this modified program are also designated as being from reference 14.

Method of Grose

An approximate inverse solution for the nonequilibrium flow in the inviscid shock layer about a vehicle in hypersonic flight is presented in reference 16. This method is based upon the flow model developed by Maslen (ref. 17) and is applicable to subsonic and supersonic regions of the shock layer. An approximation is made to the momentum equation in the direction normal to the shock that enables it to be readily integrated. From this equation the pressure distribution can be determined independently of the chemistry within the shock layer. The model of an arbitrary gas mixture permits consideration of vibrational relaxation, dissociation, recombination, ionization, electronic excitation, and vibration-dissociation coupling. The method of Grose requires specification of a shock shape and solves for the resultant body. For the present study, results from this program (ref. 16) were generated by William L. Grose for the expansion tube tests with CO_2 test gas and a 3.18-cm-radius sphere. The CO_2 model used in these calculations consisted of eight species $(CO_2, CO, C, O, O_2, O_2^+, CO^+,$ and $e^-)$ and a total of 18 reactions.

Method of Anderson and Moss

The method of reference 18 employs an implicit finite-difference scheme for the numerical solution of the viscous-shock-layer equations applicable to hypersonic laminar, transitional, and turbulent flows about blunt axisymmetric bodies. Results from this method presented herein were generated by E. C. Anderson of Old Dominion University for laminar flow. Calculations for a sphere were actually obtained by use of a spherically blunted cone having a half-angle of 45° as the geometric input; hence, the range of shock detachment distance in terms of y/r_n is limited. The perfect-gas phase of this program was exercised for helium test gas and the real-gas phase was used for air test gas. The real-air model was assumed to be argon-free and consisted of five species $(O, O_2, N, N_2,$ and $NO)$.

Method of Moss

To examine the influence of flow nonequilibrium in the shock layer on predicted shock detachment distance, the method of reference 19 was exercised for a sphere in air flow. The method of reference 19 employs an implicit finite-difference scheme to solve the viscous-shock layer equations for laminar flow. It also possesses the capability of treating the flow as being either frozen, in equilibrium, or in nonequilibrium. The effects of diffusion model, surface catalysis, and mass injection on surface transport and flow parameters are included in this method. Presented herein are equilibrium and nonequilibrium computations from the method of reference 19 for a 3.18-cm-radius sphere. These results, which were generated by James N. Moss, treat air as a mixture of five thermally perfect species $(O, O_2, N, N_2,$ and $NO)$ and assume no mass injection. The surface temperature of the sphere was varied to examine the effect of surface catalysis on shock detachment distance.

Method of Inouye

In some instances, a simple expression which provides a rapid means for estimating the shock shape is useful. Such an expression may be obtained from the results of reference 20. These results represent an extension of the calculations presented in reference 13 to include flow-field solutions for a sphere in several equilibrium gases (air, nitrogen, argon, and CO_2) and a gas mixture. Velocities from 3 to 21 km/sec were considered, and the free-stream temperature was maintained constant for each gas at a value for which the free-stream gas was undissociated. For the body-oriented coordinate system used to present data herein, the correlations of reference 20 result in the expression

$$\frac{x}{r_n} = \left[\frac{0.25\lambda^2 \left(\frac{y}{r_n}\right)^4 + A_7 \lambda^4 \left(\frac{y}{r_n}\right)^6}{1 + \frac{4A_7\lambda^4\left(\frac{y}{r_n}\right)^4}{M_1^2 - 1}} \right]^{1/2} - \frac{0.78}{\epsilon} \tag{1}$$

where, by definition,

$$\lambda \equiv \frac{1.28}{1 + \sqrt{\frac{8}{3\epsilon}}}$$

and A_7 is the shock-wave shape parameter presented in reference 20 for several equilibrium gases. For the present expansion tube air and CO_2 flow conditions, values of A_7 obtained from figure 2 of reference 20 were found to be 0.089 and 0.094, respectively. Values of A_7 for the other gases (helium, CF_4, and C_2F_6) examined are not given in reference 20.

Program of Hamilton

A program developed by Harris Hamilton of the Langley Research Center was used in the present study. This program predicts the perfect-gas inviscid flow field about blunt axisymmetric bodies in supersonic and hypersonic flows. The method of lines is used, in which the body surface is transformed from the physical plane (r,θ-plane for a sphere) to the abscissa in a rectilineal coordinate system and the bow shock is transformed to a horizontal line in this system. The region between the transformed bow shock and body surface is divided into a number of smaller regions by vertical lines in the transformed plane. Derivatives along coordinate lines parallel to the bow shock are replaced by finite-difference expressions and the resulting "ordinary" differential equations are integrated from an assumed bow shock wave toward the body. The shock shape is iterated upon until the normal components of velocity vanish at the body surface. Results designated herein as "Hamilton"

were generated by Harris Hamilton. (The method of lines procedure of Harris Hamilton has not been documented and thus the reader is referred to direct communication with Harris Hamilton for specifics of this method.) Of the various programs used herein to calculate the shock detachment distance for a sphere, the method of lines requires the least core storage and time on the computer.

RESULTS AND DISCUSSION

The measured shock shapes for a sphere presented herein were obtained in the Langley CF_4 tunnel, the Langley pilot model C_2F_6 tunnel, and the Langley expansion tube with helium, air, and carbon dioxide test gases. These five test gases may be grouped into three categories of thermodynamic behavior: (1) perfect gas such as helium, (2) near-perfect gas such as CF_4 and C_2F_6, and (3) real gas such as air and CO_2. First, a comparison of measured and predicted shock shapes for test gases exhibiting perfect gas or near-perfect gas behavior will be discussed. This discussion is followed by a similar comparison of measured and predicted shock shapes for real-gas flows (air and CO_2) and includes discussion of possible causes for observed discrepancies between measured and predicted shock shapes for these two gases.

Comparison of Measured and Predicted Shock Shapes for Near-Perfect Test Gases

Measured shock shapes for sphere models in helium, CF_4, and C_2F_6 test gases are shown in figure 1. The shaded regions of this figure denote the uncertainty in measured shock detachment distance. (This uncertainty is due to uncertainties in reading the schlieren film (ref. 1) or shadowgraph film, scatter resulting from presenting data for several runs with helium and CF_4, and small differences between readings of windward and leeward shock detachment distances.) The free-stream Mach number M_1 for these three test gases is nearly the same, whereas the normal-shock density ratio ϵ increases by a factor of four between the lowest value for helium and highest value for C_2F_6. The expected decrease in measured shock detachment distance with increasing ϵ for an essentially constant value of M_1 is illustrated in figure 1. Of the five test gases considered herein, these three (obtained from three different facilities) are divorced from real-gas effects resulting from excitation of dissociation and ionization energy modes for the present conditions; however, the CF_4 and C_2F_6 flows are not divorced from vibrational excitation. Nevertheless, thermodynamic equilibrium is assumed for CF_4 and C_2F_6. (In ref. 7, this assumption is justified for CF_4 by comparing the vibrational relaxation distances with the flow lengths.) Comparisons between measured and predicted shock shapes are discussed first for the three test gases devoid of dissociation (that is, perfect-helium and "near-perfect" CF_4 and C_2F_6).

Predictions from the methods of references 2, 3, 13, 14, and those of Hamilton are shown in figure 1 for the three test gases. (For convenience, values of x/r_n and y/r_n for the predicted shock shapes are presented in table I.) As discussed previously, the basic inputs to these methods for perfect-gas flows are Mach number and ratio of specific heats. The method of reference 14 was employed in both the perfect-gas mode and the real-gas mode. For the helium tests in the expansion tube, the ratio of specific heats is constant across the sphere bow shock (that is, γ_1 is equal to γ_2); thereby, the condition for perfect-gas flow is satisfied. However, the dependence of γ on temperature for CF_4 and C_2F_6 test gases, due to vibrational excitation, results in the ratio of specific heats in the postshock region being somewhat less than the free-stream value. To satisfy the condition of constant γ across the bow shock, effective values of specific heat ratio for CF_4 and C_2F_6 were used as input to the methods for perfect-gas flows. (As illustrated in ref. 1, measured shock shapes for a flat-faced cylinder model in air and CO_2 expansion-tube flow were in good agreement with perfect-gas predictions provided that the correct normal-shock density ratio was accounted for by using an effective value of γ.) The values of effective γ for CF_4 and C_2F_6 were determined from the perfect-gas normal-shock relation (ref. 21)

$$\gamma_{eff} = \frac{\epsilon\left(1 - \frac{2}{M_1^2}\right) + 1}{\epsilon - 1} \tag{2}$$

The results of figure 1 correspond to a relatively wide range of γ_{eff}, γ_{eff} varying from 1.067 for C_2F_6 to 1.667 for helium. For convenience, values of inputs γ_{eff} and M_1 or M_{eff} to the perfect-gas, blunt-body programs used to generate the shock shapes presented herein are as follows for the various test gases (including air and CO_2; to be discussed subsequently):

Test gas	γ_{eff}	M_{eff}
Helium	1.667	6.018
Air	1.170	8.900
CF_4	1.120	6.100
CO_2	1.091	9.937
C_2F_6	1.067	5.350

The measured helium results of figure 1(a) correspond to those presented in figure 20(a) of reference 1. Shock detachment distances predicted by references 13, 14, and by Hamilton are observed to be in good agreement with the measured helium results for the range of x/r_n, y/r_n examined, whereas the methods of references 2 and 3 underpredict the

detachment distance somewhat away from the subsonic flow region. The shock standoff distance on the center line predicted by the various methods is essentially the same. (See table I.) As discussed in references 4, 5, and 6, the effect of free-stream flow nonuniformity is to move the shock detachment distance in the stagnation region closer to the model surface and farther from the surface in the transonic and supersonic regions. The sphere is more sensitive to this phenomena than the more blunt bodies (ref. 4); hence, the sphere shock shapes were used in reference 1 to determine whether appreciable effects of flow nonuniformity exist in the expansion tube flow. The fact that comparison of measured shock shapes was made only with predicted shapes from references 2 and 3 leads to an acknowledgment in reference 1 that the helium flow may be slightly nonuniform. However, the results of figure 1(a) indicate that this implication that the helium flow may be nonuniform is unwarranted.

Measured shock detachment distances for a sphere in CF_4 and C_2F_6 flows (figs. 1(b) and 1(c), respectively) are predicted reasonably well by references 3, 13, 14, and by Hamilton, whereby the method of reference 2 is again observed to underpredict the detachment distance away from the stagnation point. It should be emphasized that the basic inputs γ_{eff} and M_1 to these methods were identical and the time parameter for the unsteady computational scheme of reference 2 was varied to insure a steady-state (time-asymptotic) solution.

The results of figure 1 demonstrate that over a wide range of ratios of specific heat, the methods of references 13 and 14 provide accurate predictions of measured shock detachment distance over the range of $x/r_n, y/r_n$ of interest. At the lower values of the ratios of specific heat, the method of reference 3 also provides accurate shock shape predictions and is attractive from the viewpoint that it requires less computer time than required by the methods of references 13 and 14. The method of lines solution of Hamilton is also attractive, since it provides good agreement with measured shock shapes for the range of density ratio considered and requires even less computer time than the method of reference 3. However, at the time of this study, the range of application was limited in terms of x/r_n and y/r_n.

Since values of the shock-wave-shape parameter A_7 required in equation (1) are not given in reference 20 for helium, CF_4, or C_2F_6, an iteration on A_7 was performed to yield the best shock shape fit with experiment for these three gases. This iteration yielded values of A_7 equal to 0, 0.63, and 0.55, respectively, for helium, CF_4, and C_2F_6. The value of A_7 equal to zero for helium implies the shock shape may be estimated by the expression

$$\frac{x}{r_n} = \left[0.64\left(\frac{y}{r_n}\right)^2 \Big/ \left(1 + \sqrt{\frac{8}{3\epsilon}}\right)\right] - \frac{0.78}{\epsilon}$$

which depends only on the normal shock density ratio or Mach number for a perfect gas. Naturally, the present values of A_7 for CF_4 and C_2F_6 are not general and should be applied only to the flow conditions presented herein for the CF_4 tunnel and pilot model C_2F_6 tunnel.

Comparison of Measured and Predicted Shock Shapes for Real Gases

Measured values of shock detachment distance for a sphere in air and CO_2 flows are presented in figure 2. These results, which were obtained in the Langley expansion tube and are illustrated in figure 20 of reference 1, are compared with predictions from references 2, 3, 13, 14, 20, and by Hamilton. The shaded region represents uncertainty in measured values of shock detachment distance. Since real-gas effects for these measurements are very large for both test gases, the methods of references 2, 13, and 14 were exercised in both a perfect-gas mode and a real-gas mode. For the perfect-gas mode of references 2, 13, and 14 as well as for the method of reference 3 and Hamilton, the basic inputs were effective ratios of specific heat and effective Mach number. (The procedure for determining M_{eff} and the use of M_{eff} as opposed to M_1 are discussed in ref. 1.) Basic inputs to the real-gas mode of references 2, 13, and 14 were free-stream density ρ_1, static pressure p_1, and free-stream velocity U_1.

Comparison of measured and predicted shock detachment distances for air and CO_2 (fig. 2) shows that all theoretical methods considered underpredict the measured detachment distance. This underprediction of shock detachment distance is observed for both the perfect-gas and real-gas methods. Comparing the perfect-gas with the real-gas predictions for reference 2, reference 13, and reference 14 shows the calculated detachment distance for real air is only slightly greater than that for perfect air with inputs γ_{eff} and M_{eff}; the real CO_2 and perfect CO_2 predictions of detachment distance from reference 13 and from reference 14 are essentially the same. This comparison demonstrates that no appreciable loss of accuracy in predicted detachment distance occurs when simple perfect-gas relations with effective ratio of specific heat input are used in place of methods requiring real-gas, equilibrium thermodynamic properties. This result is significant, since perfect-gas relations greatly simplify the computational procedure for determining the flow characteristics about hypersonic blunt bodies where real-gas effects are appreciable. (Comparison of perfect-gas (inputs γ_{eff} and M_{eff}) and real-gas predicted pressure distributions about a sphere, using the methods of ref. 13 and ref. 14, showed the two predictions from each method to be nearly identical for air and for CO_2.) As observed for CF_4 and C_2F_6 test gases (fig. 1), shock

detachment distances predicted from reference 2 are significantly less than the other predictions away from the stagnation region.[1]

That measured detachment distances for air and CO_2 exceed prediction may be attributed to any one of several causes or combinations of these causes. One is that the prediction methods of references 2, 3, 13, 14, and Hamilton do not include the shock displacement from the sphere surface which may result from appreciable viscous (boundary-layer displacement thickness) effects. A second is that the methods discussed to this point do not include the effects of chemical nonequilibrium within the shock layer. A third reason for discrepancy between measured and predicted detachment distance may be due to uncertainties in predicted expansion-tube flow quantities. (As discussed in ref. 22, an accurate determination of flow conditions in impulse facilities is often difficult. Naturally, uncertainties in predicted expansion tube air and CO_2 flow conditions will result in corresponding uncertainties in predicted detachment distance.) A fourth cause may be free-stream flow-nonuniformity effects as discussed in reference 1. A fifth possible contributing factor to the observed discrepancy for air and CO_2 results may be due to the flow establishment process about the sphere model. In the expansion tube flow sequence, the test model is subjected to the high-velocity low-density acceleration gas flow prior to the test gas flow. Thus, the shock layer and boundary layer on the model surface must adjust to the change in flow conditions resulting from the arrival of the acceleration-gas-test-gas interface at the model. The time required for the test gas to "wipe" the acceleration gas from the model flow field is of primary interest, because of the short expansion tube test times of 200 to 250 μsec. Since these possible contributors to the discrepancy between measured and predicted shock shapes are common, hence of concern, to most hypervelocity impulse facilities, each will now be discussed in some detail.

Effect of uncertainties in predicted shock shapes.- The effect of uncertainties in predicted expansion tube flow conditions is discussed first. These flow conditions were calculated by using nominal values of measured wall (free-stream) pressure, free-stream velocity, and stagnation pressure behind a normal shock as inputs to the program of reference 23. Combinations of the expected maximum uncertainty in each of these measured inputs were examined.

[1]After the completion of this study, both the method of reference 2 and method of reference 4 were exercised by Richard W. Barnwell in the perfect-gas mode to predict the shock shape for a sphere in uniform flow. Identical inputs were employed, the effective ratio of specific heats being 1.17, corresponding to the present air results. The shock shape predicted from reference 4 was observed to be in good agreement with those predicted by using the methods of references 13 and 14; however, the shock detachment distance predicted by using reference 2 was significantly less than these other predicted detachment distances, particularly in the supersonic flow region about the sphere. Also, the behavior of the computations from the method of reference 2 looked suspicious. Thus, past and future users of the method of reference 2 are cautioned to use this method with discretion, particularly for low values of specific heat ratio and for blunt bodies having an appreciable portion of their flow field in the supersonic regime.

Those combinations yielding the maximum uncertainties in the corresponding value of normal-shock density ratio (that is, combinations yielding the minimum and maximum value of ϵ) were sought to generate corresponding uncertainties in shock detachment distance. (Maximum and minimum values of ϵ were sought in the present error analysis since ϵ is the primary factor governing the shock detachment distance of blunt bodies at hypersonic speeds.) Based on the results of figure 1, the perfect-gas mode of reference 13 was accepted as the best method (in view of accuracy and computer time requirements) to calculate the shock shapes corresponding to these extremes in ϵ. (The method of ref. 13 was chosen over the method of ref. 14 only because it required less computer time per case.)

The results of this uncertainty analysis are shown in figure 3 for helium, air, and CO_2 test gases. For helium, γ_{eff} is equal to 1.667 and the minimum and maximum values in Mach number $(M_{eff}$ equal to $M_1)$, resulting from uncertainties in measured inputs, correspond to the minimum and maximum values in normal-shock density ratio, respectively. Similarly, input combinations for CO_2 yielding the maximum value of ϵ also yielded the maximum values of M_{eff} and γ_{eff}; however, for air, the maximum value of ϵ does not correspond to maximum values of M_{eff} and γ_{eff}. In this case, the uncertainty in shock detachment distance corresponding to the range of uncertainty in input γ_{eff} for a given value of M_{eff} was used. (See fig. 3(b).) From figure 3(a), the regions of uncertainty corresponding to predicted shock detachment distance and to measured detachment distance essentially overlap for the helium test gas. In general, the region of uncertainty corresponding to predicted detachment distance for air and CO_2 (figs. 3(b) and 3(c)) lies closer to the model surface than the region of uncertainty for measured detachment distance. Since the same instrumentation was used to measure inputs p_1, p_t, and U_1 for all three test gases, and the magnitude of each input was of the same order for each gas, uncertainties in measured inputs are expected to be essentially the same for these gases. However, in calculating flow conditions by using the program of reference 23, the assumption of free-stream and post-bow-shock thermochemical equilibrium is made. This assumption is, of course, valid for the present helium flow conditions, but questionable for air and CO_2 (ref. 24). Experimental uncertainties used herein for measured p_1 and p_t are believed to be realistic, since time histories for these quantities were measured and reported in reference 1. Time histories of U_1 were not measured, and as illustrated in reference 25, variations in U_1 were observed in the Langley pilot model expansion tube with time. However, increasing the uncertainty in input U_1 by a factor of two (representing the maximum uncertainty in U_1 reported in ref. 25) does not result in a significant variation to γ_{eff} and M_{eff} for air and CO_2. (See fig. 17 of ref. 1.) Also, the flat-faced cylinder results of reference 1 imply the free-stream flow for air and CO_2 is close to thermochemical equilibrium. Although uncertainties in calculated flow conditions may contribute to the observed discrepancy between measured and predicted shock shapes for air and CO_2, attributing this discrepancy only to such uncertainties is not believed to be justified.

Effect of viscosity.- At sufficiently low Reynolds numbers, the shock thickness and boundary-layer thickness are no longer negligible compared with the shock detachment distance, and the shock detachment distance for hypersonic blunt bodies becomes a function of Reynolds number as well as normal-shock density ratio. In this regime, the shock detachment distance increases with decreasing Reynolds number. The assumption was made in reference 1 that the shock standoff distance for the present air and CO_2 sphere tests was independent of Reynolds number (viscous) effects. This was based on the fact that the helium sphere data, which were divorced from possible effects of flow chemistry, showed the shock standoff distance to be essentially constant with Reynolds number (based on post-normal-shock flow conditions and sphere diameter) for values greater than 2×10^3. Also, the argon results of reference 26 imply the absence of a Reynolds number effect for values of $N_{Re,2,d_n}$ in excess of 1×10^3. Since the Reynolds number $N_{Re,2,d_n}$ for the present air and CO_2 test gas results is close to 2×10^4, the shock detachment distance should be independent of $N_{Re,2,d_n}$. The ratio of model wall temperature to stagnation point temperature $T_w/T_{t,2}$ influences the detachment distance, detachment distance increasing with increasing $T_w/T_{t,2}$ (ref. 26). For the present results, $T_w/T_{t,2}$ for helium, air, and CO_2 are relatively small (0.06, 0.05, and 0.08, respectively, in the early portion of the test flow period, and not expected to increase drastically (for example, double) during the entire test period); thereby the effect of temperature ratio on shock detachment distance is diminished.

The assumption of negligible viscous effects was also examined by using the method of reference 18 to compute the boundary-layer displacement thickness for a sphere at the present helium and air test conditions. The boundary layer was assumed to be laminar. For the helium flow, calculated displacement thickness normal to the model surface was less than 2 percent of the calculated shock detachment distance normal to the model for the range of $x/r_n, y/r_n$ for which the program of reference 18 is applicable. (See table I.) For real-air flow, the calculated displacement thickness was approximately 1 percent of the shock detachment distance for the range of $x/r_n, y/r_n$ examined. Hence, the assumption of essentially negligible viscous effects for the present shock detachment distances appears to be justified.

Effect of flow nonuniformity.- In general, the effect of flow nonuniformity, in which the free-stream velocity decreases with radial distance from the tube or nozzle center line, is to move the shock detachment distance in the stagnation region (subsonic region) closer to the body and farther from the body in the supersonic region. (See refs. 4, 5, and 6.) Comparisons of measured and predicted (refs. 2 and 4) shock shapes for a sphere in reference 1 indicated that the helium flow may be slightly nonuniform and the air and CO_2 flows are probably nonuniform. As noted in reference 1, the uncertainty associated with the prediction of the shock detachment distance away from the stagnation region for a sphere in air and CO_2 test gases, using perfect-gas relations with M_{eff} and γ_{eff} inputs, prohibited a definite conclusion concerning flow nonuniformity. The present results have demonstrated

that inputs M_{eff} and γ_{eff} yield shock detachment distances that are in good agreement with those predicted with real-gas solutions; thereby, the reason given in reference 1 for prohibiting a conclusion concerning flow nonuniformity is removed.

Implication of possible flow nonuniformity in reference 1 resulted from comparison of measured shock shapes for a sphere to predicted values of references 2 and 4. The fact that the measured detachment distance exceeded these predictions for uniform flow and agreement was improved significantly by the inclusion of free-stream flow nonuniformity in the predictions led to this implication. However, the results of figure 1 for helium, CF_4, and C_2F_6 test gases illustrate the method of reference 2 underpredicts the shock detachment distance away from the stagnation region in comparison to the other predictions and measurement. This discrepancy between the results of reference 2 and the other predictions increases with increasing normal shock density ratio. Thus, the use of reference 2 to deduce the existence of flow nonuniformity in reference 1 appears to be unfortunate.

The good agreement between experiment and the predictions of references 13 and 14 for helium (fig. 1(a)) indicates near uniform free-stream helium flow in the expansion tube. The air and CO_2 results were generated in the same facility as the helium results, the only difference between tests being the test gases and acceleration gases employed and the quiescent acceleration gas pressure. Free-stream pressures and velocities and stagnation-point pressures were the same order of magnitude for these test gases. Hence, it appears reasonable to assume flow uniformity for all three test gases is similar. (It should be noted, however, that differences do exist between helium flow in the Langley expansion tube and air and CO_2 flows (ref. 1). Consequently, the absence of a mechanism for generating nonuniform helium flow does not necessarily imply an absence of such a mechanism for air and CO_2 flows.)

In the following table, the ratio of measured shock detachment distance normal to the sphere surface to predicted detachment distance from the real-gas program of reference 13 is presented for air and CO_2 for various values of angle θ:

Air		CO_2	
θ, deg	δ_m/δ_{pr}	θ, deg	δ_m/δ_{pr}
0	1.08	0	1.20
5	1.09	4.5	1.20
10	1.12	9.5	1.24
15.5	1.15	14.5	1.30
21	1.18	20	1.30
26	1.16	25	1.31
31.5	1.19	30	1.36
37	1.19	35.5	1.36
43.5	1.22	41.5	1.35
49.5	1.23	47.5	1.30
55.5	1.23	54.0	1.25
62.5	1.22	60.5	1.24
69	1.22	67.5	1.25

These values are approximate because of the relatively large uncertainty in measured detachment distance. In general, the ratio of measured detachment distance to predicted detachment distance for both air and CO_2 increases away from the stagnation point. Further downstream, the ratio remains essentially constant for air and decreases somewhat for CO_2. In figure 4, the ratio of measured detachment distance to predicted (ref. 13) detachment distance for air is shown as a function of the angle θ. Also shown in this figure is the ratio of detachment distance predicted for nonuniform free-stream flow to detachment distance predicted for uniform free-stream flow. These predictions were generated by Richard W. Barnwell (refs. 2 and 4) in support of the study of reference 1. The nonuniform free-stream flow model used in reference 4 assumed a parabolic variation in free-stream velocity with perpendicular distance from the model axis. The quantity λ shown in figure 4 denotes the percent deviation of free-stream velocity at a distance from the tube center line equal to the sphere radius. Free-stream static pressure and total enthalpy are assumed in reference 4 to be constant. Ratios for values of λ equal to 1, 3, 6, and 10 percent are presented in figure 4. As observed from this figure, the experimental shock detachment distance does not move closer to the sphere surface in the subsonic region of the shock layer as predicted by reference 4. In the fully supersonic region within the shock layer, a 1-percent variation in free-stream velocity in reference 4 is observed to yield higher values of shock detachment distance ratio than experiment. Similar discrepancies between experiment and the nonuniform predictions of reference 4 were observed for CO_2 test gas. The results of these comparisons coupled with the good agreement between experiment and prediction for helium test gas tend to preclude the existence of free-stream flow nonuniformity for air and CO_2, in which the free-stream velocity decreases radially from the tube center line. However, additional flow diagnostics, such as the technique reported in reference 25 for measuring radial free-stream velocity profiles, are required to substantiate the absence of flow nonuniformity in the expansion tube at the present air and CO_2 test conditions.

Effect of flow establishment.- For helium, air, and CO_2 test gases, the time interval between arrival of the incident shock in the acceleration gas (which is the same gas as the test gas for the present tests) at the model and the subsequent arrival of the acceleration-gas–test-gas interface is 25 to 30 microseconds. Hence, the model is subjected to supersonic flow characterized by relatively high free-stream temperatures and low free-stream densities prior to the arrival of the test gas. According to the predictions of references 27 and 28, the time required for the unsteady shock detachment distance for a sphere to become within a few percent of the steady-state value for the acceleration gas flow conditions is less than the time interval between the incident shock and interface. Hence, upon arrival at the model, the test gas will (according to prediction) encounter a quasi-steady flow already established about the model. Although the acceleration gas and test gas are the same, the thermodynamic states of these gases are very different. For example, the free-stream density in the acceleration gas for air tests is roughly one-fifth the free-stream density in the test air. Since the static

pressure is assumed to be constant across the interface, the free-stream temperature in the acceleration air is roughly 5 times that in the test air. Predicted shock standoff distance at the sphere center line for the acceleration air is 1.34 times that for test air. Since the Reynolds number for acceleration air is only 0.06 times that for test air and the scaling law parameter (product of free-stream density and shock standoff distance) is only 0.24 times that for test air, viscous effects and nonequilibrium effects are more severe for the acceleration gas phase of the flow. Hence, for air, the ratio of standoff distance for acceleration air to test air of 1.34 should be conservative. A similar analysis for CO_2 shows the difference between standoff distance for acceleration flow and test flow to be greater than that for air, the ratio between the two being roughly 2.1. Attempts to obtain time histories of the bow shock development over the sphere in air and CO_2 flows with a high-speed framing camera during the tests reported in reference 1 were only partially successful. Poor shock resolution on the enlargements of each film frame and off-axis alinement for this system prohibited accurate determination of the center-line shock standoff distance. Hence, it was not determined experimentally whether sufficient run time existed for the test flow to fully "wipe off" the acceleration flow from over the sphere model. Residual acceleration gas flow over the model would tend to result in a greater shock. detachment distance than expected for the test-gas flow.

The time required for the acceleration-gas boundary layer and inviscid flow to relax to the test-gas boundary layer and inviscid flow over a flat plate has been treated theoretically in reference 29. A steady-state boundary layer containing more than 95 percent of the test gas ("perfect" nitrogen) was predicted to exist over a plate length equal to three-tenths of the distance traveled by the interface from the leading edge of the flat plate. That is, for a plate length corresponding to the distance traveled by the air interface during the 200 microsecond quasi-steady test period (1.06 m), essentially all the acceleration gas flow in the first 0.32 meter of the plate have relaxed to the test-gas flow. By considering (1) the present sphere diameter is only 1/50 of the approximate predicted length required for the test flow to replace the acceleration flow on a flat plate, (2) the schlieren spark source was fired 140 to 180 microseconds into the test flow, and (3) viscous flow, which relaxes more slowly than inviscid flow, is less of a contributor to the flow field for a sphere than for a flat plate, the assumption that a quasi-steady shock detachment distance for the sphere exists in the test gas flow appears to be feasible. (It should be noted that the predictions of ref. 29 are idealized in many respects and have not been verified experimentally.)

Unreported time histories of the measured heat-transfer rate to the surface of a flat-faced cylinder for the present air and helium flow conditions demonstrate that quasi-steady values of heat transfer rate are obtained approximately 90 and 60 microseconds, respectively, after arrival of the incident shock in the acceleration gas. Since the flow establishment time for a sphere is more rapid than that for a flat-faced cylinder of the same radius, these heat-transfer

results also infer that a quasi-steady shock detachment distance should exist for the sphere during the test-gas flow period.

Effect of flow nonequilibrium.- The effect of flow nonequilibrium within the shock layer of the sphere model for air and CO_2 test gases was discussed in some detail in reference 1. The results of reference 1 showed that the measured ratio of shock standoff distance to nose radius decreased monotonically with increasing sphere diameter toward the predicted shock standoff distance. For the largest sphere diameter tested (7.62 cm), the measured standoff distance for air and CO_2 was roughly 1.08 and 1.2 times the predicted standoff distance. Since the effect of free-stream flow nonuniformity has a relatively small effect on, and tends to decrease, the shock standoff distance and viscous effects were deduced to be negligible, this variation for air and CO_2 was attributed in reference 1 to nonequilibrium flow in the shock layer.

To examine this departure from equilibrium further, the nonequilibrium programs of reference 19 and reference 16 were used to calculate the shock detachment distance for a 3.18-cm-radius sphere at the present air and CO_2 test conditions, respectively. The results of these calculations are compared with measured shock detachment distance for these two test gases in figure 5. Also shown in figure 5 are shock shapes calculated by using the thermochemical equilibrium program of reference 14. These predictions of reference 14 are deemed as "benchmark" equilibrium solutions and presented for comparison. For air (fig. 5(a)), the equilibrium predictions of references 14 and 19 are observed to be in good agreement and, as expected, underpredict the measured detachment distance. However, inclusion of nonequilibrium effects in the method of reference 19 yields good agreement between measured and predicted detachment distance for air test gas. The predicted increase in detachment distance for nonequilibrium flow, using the method of reference 19, is attributed to chemistry only since the flow model used in the two computations is the same. Variation in model surface temperature from 300 K to 1000 K in the nonequilibrium prediction of reference 19 did not produce an appreciable effect on calculated shock detachment distance.

For CO_2 (fig. 5(b)), the shock detachment distance predicted by using the method of reference 17 (and generated by Walter B. Olstad of the Langley Research Center for the present study) is observed to be significantly less than the detachment distance predicted by using the method of reference 14. This comparison is made since the nonequilibrium method of reference 16 utilizes the flow model of reference 17. Because the flow model developed in reference 17 underpredicts the shock detachment distance for equilibrium flow, it is presumed to also underpredict the detachment distance for flows with nonequilibrium chemistry. Hence, a correction factor equal to the ratio of the detachment distance predicted by using the method of reference 14 to that predicted by using reference 17, for given values of θ, was applied to the nonequilibrium shock shape predicted by reference 16. These

correction factors ranged from approximately 1.12 to 1.25 for values of θ to 60°. As observed from figure 5(b), the corrected shock detachment distance predicted for nonequilibrium CO_2 is in good agreement with measured detachment distance. Based on these comparisons in figure 5, the primary cause of the observed discrepancy between measured and predicted shock detachment distance in figure 2 for air and CO_2 test gases is the existence of nonequilibrium flow within the shock layer for the 3.18-cm-radius sphere. To attain equilibrium flow over a sphere model in the Langley expansion tube for air and CO_2 test gases at hypersonic conditions, the free-stream density must be increased. (The 3.18-cm-radius sphere model has nearly the same radius as the inviscid test core for both test gases; hence, to increase the scaling law parameter (product of free-stream density and shock standoff distance) into the near-equilibrium flow regime, the free-stream density must be increased. (See fig. 34 of ref. 1.)

CONCLUDING REMARKS

Measured shock shapes for sphere and hemisphere models in helium, air, CF_4, C_2F_6, and CO_2 test gases corresponding to normal-shock density ratios from 4 to 19 are presented. These shock shapes were obtained in three facilities at the Langley Research Center capable of generating the high density ratios experienced during planetary entry at hypersonic conditions, namely the 6-inch expansion tube, the CF_4 tunnel, and the pilot CF_4 Mach 6 tunnel $\left(\text{with } CF_4 \text{ replaced by } C_2F_6\right)$. Comparison of the measured results with several methods for predicting inviscid, perfect-gas shock detachment distance and to real-gas predictions which include effects of a laminar viscous layer and thermochemical nonequilibrium is performed.

With the exception of one prediction method, good agreement was observed between measured shock detachment distances from the three facilitites, with respective test gases helium, CF_4, and C_2F_6, and the various prediction methods examined. These three test gases exhibit near-perfect gas behavior and provide a normal-shock density range from 3.7 to 15.1. The one exception (method of NASA TN D-6283) underpredicted detachment distance, this underprediction worsening with increasing density ratio.

Measured detachment distance for air and CO_2 obtained in the expansion tube exceeded prediction. Comparison of the various predictions for air and CO_2 showed detachment distance predicted by using real-air programs was only slightly greater than those predicted by using simple, perfect-air relations with effective ratio of specific heats and effective Mach number as inputs; for CO_2, real CO_2 and perfect CO_2 predictions of detachment distance were essentially the same. Therefore, the detachment distance for real-gas flows may be accurately predicted by using perfect gas programs with substantial savings in computer time.

A number of possible explanations for the discrepancy between measured and predicted detachment distance in air and CO_2 are discussed in some detail, since these topics are of

concern in hypervelocity, impulse facility testing. The primary cause of the observed discrepancy is attributed to thermochemical nonequilibrium within the shock layer. This conclusion is the result of comparison of measured shock detachment distance to predictions accounting for nonequilibrium flow for both air and CO_2. Viscous effects are deduced to be small, the model boundary-layer displacement thickness not exceeding 2 percent of the shock-layer thickness. The maximum uncertainties in predicted flow conditions for air and CO_2 do not yield corresponding uncertainties in predicted detachment distance large enough to attribute the discrepancy solely to such uncertainties. The test-gas flow is assumed to "wipe off" the previously established acceleration gas flow from the sphere flow field. (The shock standoff distance for the acceleration-gas flow period is substantially greater than that for the test flow period.) The measured detachment distances for air and CO_2 do not follow the trends predicted for nonuniform free-stream flow; also, the helium results obtained in the same facility do not exhibit effects of flow nonuniformity. Hence, possible effects of flow nonuniformity for air and CO_2 are not believed to be significant.

National Aeronautics and Space Administration
Langley Research Center
Hampton, Va. 23665
September 16, 1975

REFERENCES

1. Miller, Charles G., III: Shock Shapes on Blunt Bodies in Hypersonic-Hypervelocity Helium, Air, and CO_2 Flows, and Calibration Results in Langley 6-Inch Expansion Tube. NASA TN D-7800, 1975.
2. Barnwell, Richard W.: A Time-Dependent Method for Calculating Supersonic Angle-of-Attack Flow About Axisymmetric Blunt Bodies With Sharp Shoulders and Smooth Non-axisymmetric Blunt Bodies. NASA TN D-6283, 1971.
3. Zoby, Ernest V.; and Graves, Randolph A., Jr.: A Computer Program for Calculating the Perfect Gas Inviscid Flow Field About Blunt Axisymmetric Bodies at an Angle of Attack of 0°. NASA TM X-2843, 1973.
4. Barnwell, Richard W.: A Time-Dependent Method for Calculating Supersonic Blunt-Body Flow Fields With Sharp Corners and Embedded Shock Waves. NASA TN D-6031, 1970.
5. Patterson, Jerold L.; and Lewis, Arthur B.: An Investigation of Nonuniform Hypersonic Free-Stream Flows About Blunt Axisymmetric Bodies. AFFDL-TR-69-57, U.S. Air Force, Nov. 1969. (Available from DDC as AD 700 984.)
6. Inouye, Mamoru: Numerical Solutions for Blunt Axisymmetric Bodies in a Supersonic Spherical Source Flow. NASA TN D-3383, 1966.
7. Jones, Robert A.; and Hunt, James L. (With appendix A by James L. Hunt, Kathryn A. Smith, and Robert B. Reynolds, and appendix B by James L. Hunt and Lillian R. Boney): Use of Tetrafluoromethane To Simulate Real-Gas Effects on the Hypersonic Aerodynamics of Blunt Vehicles. NASA TR R-312, 1969.
8. Jones, Robert A.; and Hunt, James L.: Measured Pressure Distributions on Large-Angle Cones in Hypersonic Flows of Tetrafluoromethane, Air, and Helium. NASA TN D-7429, 1973.
9. Hunt, James L.; Jones, Robert A.; and Smith, Kathryn A.: Use of Hexafluoroethane To Simulate the Inviscid Real-Gas Effects on Blunt Entry Vehicles. NASA TN D-7701, 1974.
10. Moore, John A.: Description and Initial Operating Performance of the Langley 6-Inch Expansion Tube Using Heated Helium Driver Gas. NASA TM X-3240, 1975.
11. Trimpi, Robert L.: A Preliminary Theoretical Study of the Expansion Tube, A New Device for Producing High-Enthalpy Short-Duration Hypersonic Gas Flows. NASA TR R-133, 1962.
12. Barnwell, Richard W.; and Davis, Ruby M.: A Computer Program for Calculating Inviscid, Adiabatic Flow About Blunt Bodies Traveling at Supersonic and Hypersonic Speeds at Angle of Attack. NASA TM X-2334, 1971.

13. Lomax, Harvard; and Inouye, Mamoru: Numerical Analysis of Flow Properties About Blunt Bodies Moving at Supersonic Speeds in an Equilibrium Gas. NASA TR R-204, 1964.

14. Sutton, Kenneth: Characteristics of Coupled Nongray Radiating Gas Flows With Ablation Product Effects About Blunt Bodies During Planetary Entries. Ph. D. Thesis, North Carolina State Univ. at Raleigh, 1973. (Available as NASA TM X-72078.)

15. Sutton, Kenneth: Fully Coupled Nongray Radiating Gas Flows With Ablation Product Effects About Planetary Entry Bodies. AIAA Paper No. 73-672, July 1973.

16. Grose, William L. (With appendix A by Barbara L. Weigel): A Thin-Shock-Layer Solution for Nonequilibrium, Inviscid Hypersonic Flows in Earth, Martian, and Venusian Atmospheres. NASA TN D-6529, 1971.

17. Maslen, S. H.: Inviscid Hypersonic Flow Past Smooth Symmetric Bodies. AIAA J., vol. 2, no. 6, June 1964, pp. 1055-1061.

18. Anderson, E. C.; and Moss, James N.: Numerical Solution of the Hypersonic Viscous-Shock-Layer Equations for Laminar, Transitional, and Turbulent Flows of a Perfect Gas Over Blunt Axially Symmetric Bodies. NASA TN D-7865, 1975.

19. Moss, James N.: Reacting Viscous-Shock-Layer Solutions With Multicomponent Diffusion and Mass Injection. NASA TR R-411, 1974.

20. Inouye, Mamoru: Blunt Body Solutions for Spheres and Ellipsoids in Equilibrium Gas Mixtures. NASA TN D-2780, 1965.

21. Ames Research Staff: Equations, Tables, and Charts for Compressible Flow. NACA Rep. 1135, 1953. (Supersedes NACA TN 1428.)

22. Miller, Charles G., III; and Wilder, Sue E.: Real-Air Data-Reduction Procedures Based on Flow Parameters Measured in the Test Section of Supersonic and Hypersonic Facilities. NASA TN D-6618, 1972.

23. Miller, Charles G., III: Computer Program of Data Reduction Procedures for Facilities Using CO_2-N_2-O_2-Ar Equilibrium Real-Gas Mixtures. NASA TM X-2512, 1972.

24. Haggard, Kenneth V.: Free-Stream Temperature, Density, and Pressure Measurements in an Expansion Tube Flow. NASA TN D-7273, 1973.

25. Friesen, Wilfred J.: Use of Photoionization in Measuring Velocity Profile of Free-Stream Flow in Langley Pilot Model Expansion Tube. NASA TN D-4936, 1968.

26. Bailey, A. B.; and Sims, W. H.: The Shock Shape and Shock Detachment Distance for Spheres and Flat-Faced Bodies in Low-Density, Hypervelocity, Argon Flow. AEDC-TDR-63-21, U.S. Air Force, Feb. 1963.

27. Syshchikova, M. P.; Berezkina, M. K.; and Semenov, A. N.: Formation of Frontal Shock Waves at Blunt Bodies in Shock Tubes. Soviet Phys.-Tech. Phys., vol. 9, no. 11, May 1965, pp. 1549-1553.

28. Barnwell, Richard W.: Numerical Results for the Diffraction of a Normal Shock Wave by a Sphere and for the Subsequent Transient Flow. NASA TR R-268, 1967.

29. Gupta, Roop N.: An Analysis of the Relaxation of Laminar Boundary Layer on a Flat Plate After Passage of an Interface With Application to Expansion-Tube Flows. NASA TR R-397, 1972.

TABLE I.- PREDICTED SHOCK SHAPES FOR A SPHERE IN HYPERSONIC HELIUM, CF_4, C_2F_6, AIR AND CO_2 FLOWS

(a) Values based on references 2 and 12 (Barnwell)

Predicted shock shapes for –											
Helium (ideal)		Air (ideal)		Air (real)		CF_4 (ideal)		C_2F_6		CO_2 (ideal)	
x/r_n	y/r_n	x/r_n	y/r_n	x/r_n	y/r_n	x/r_n	y/r_n	x/r_n	y/r_n	x/r_n	y/r_n
-0.217	0	-0.074	0	-0.076	0	-0.068	0	-0.057	0	-0.042	0
-.204	.159	-.060	.140	-.063	.140	-.055	.139	-.044	.137	-.038	.137
-.184	.317	-.042	.279	-.045	.280	-.037	.278	-.026	.275	-.008	.270
-.136	.471	.006	.412	.002	.413	.011	.410	-.022	.405	.037	.399
-.086	.627	.068	.533	.063	.541	.072	.536	.033	.530	.098	.521
-.006	.772	.143	.658	.137	.662	.146	.655	.156	.648	.172	.636
.087	.913	.230	.770	.223	.777	.232	.768	.242	.758	.258	.742
.193	1.051	.323	.876	.322	.834	.330	.873	.339	.862	.356	.839
.315	1.186	.437	.975	.431	.985	.438	.973	.446	.960	.463	.930
		.557	1.069	.552	1.082	.558	1.068	.564	1.053	.581	1.011
		.689	1.160	.685	1.176	.689	1.161	.693	1.145	.708	1.090
		.835	1.250	.833	1.271	.835	1.253	.837	1.237	.846	1.173

(b) Values based on reference 3 (Zoby and Graves)

Predicted shock shapes for –									
Helium (ideal)		Air (ideal)		CF_4 (ideal)		C_2F_6 (ideal)		CO_2 (ideal)	
x/r_n	y/r_n	x/r_n	y/r_n	x/r_n	y/r_n	x/r_n	y/r_n	x/r_n	y/r_n
-0.216	0	-0.071	0	-0.065	0	-0.053	0	-0.043	0
-.207	.165	-.070	.079	-.062	.079	-.051	.068	-.041	.057
-.179	.327	-.060	.157	-.054	.157	-.045	.136	-.037	.114
-.134	.486	-.047	.235	-.041	.235	-.035	.204	-.029	.171
-.073	.639	-.028	.312	-.023	.311	-.021	.271	-.019	.228
.004	.785	-.005	.337	.000	.386	-.003	.337	-.006	.284
.095	.923	.023	.461	.028	.460	.018	.402	.010	.339
.165	1.012	.059	.542	.064	.541	.051	.482	.038	.418
.248	1.107	.099	.615	.105	.616	.085	.553	.064	.478
.339	1.201	.152	.699	.157	.699	.134	.638	.108	.563
		.212	.781	.218	.782	.187	.718	.146	.628
		.282	.864	.239	.865	.251	.800	.195	.698
		.362	.947	.370	.949	.324	.883	.251	.769
		.455	1.031	.463	1.034	.409	.966	.317	.842
		.560	1.115	.570	1.119	.506	1.049	.393	.915
		.681	1.199	.692	1.200	.617	1.134	.479	.489
						.744	1.218	.577	1.063
								.689	1.137
								.816	1.213

TABLE I.- Continued

(c) Values based on reference 13 (Lomax and Inouye)

Predicted shock shapes for –													
Helium (ideal)		Air (ideal)		Air (real)		CF_4 (ideal)		C_2F_6 (ideal)		CO_2 (ideal)		CO_2 (real)	
x/r_n	y/r_n	x/r_n	y/r_n	x/r_n	y/r_n	x/r_n	y/r_n	x/r_n	y/r_n	x/r_n	y/r_n	x/r_n	y/r_n
-0.217	0	-0.071	0	-0.071	0	-0.066	0	-0.053	0	-0.043	0	-0.043	0
-.216	.056	-.070	.047	-.071	.048	-.065	.047	-.052	.046	-.042	.045	-.042	.044
-.213	.112	-.067	.094	-.068	.096	-.062	.094	-.050	.092	-.039	.089	-.039	.088
-.208	.168	-.062	.141	-.063	.144	-.057	.141	-.045	.139	-.035	.134	-.035	.133
-.200	.224	-.055	.188	-.056	.192	-.051	.188	-.039	.185	-.029	.178	-.028	.177
-.191	.280	-.047	.235	-.047	.240	-.042	.235	-.030	.231	-.020	.223	-.020	.221
-.179	.336	-.036	.282	-.037	.277	-.031	.282	-.020	.277	-.010	.267	-.010	.265
-.165	.392	-.024	.329	-.024	.335	-.019	.329	-.007	.323	.002	.312	.002	.309
-.149	.448	-.009	.377	-.009	.383	-.004	.377	.007	.370	.016	.356	.015	.354
-.131	.504	.008	.424	.008	.431	.013	.424	.023	.416	.032	.401	.031	.398
-.111	.560	.027	.471	.027	.479	.031	.471	.042	.462	.050	.446	.049	.442
-.088	.616	.048	.518	.049	.527	.052	.518	.063	.508	.070	.490	.069	.486
-.063	.672	.071	.565	.073	.575	.076	.565	.086	.554	.092	.535	.091	.530
-.035	.728	.097	.612	.099	.623	.102	.612	.111	.600	.117	.579	.116	.575
-.005	.784	.125	.659	.128	.671	.130	.659	.139	.647	.144	.624	.143	.619
.027	.840	.156	.706	.159	.718	.160	.706	.169	.693	.174	.668	.172	.663
.062	.896	.189	.753	.193	.766	.193	.753	.201	.739	.207	.713	.204	.707
.099	.952	.226	.800	.229	.814	.229	.800	.237	.785	.242	.757	.239	.752
.139	1.008	.264	.847	.269	.862	.268	.847	.775	.831	.279	.802	.277	.796
.182	1.064	.306	.894	.311	.910	.309	.894	.315	.877	.320	.847	.317	.840
.227	1.120	.351	.941	.357	.958	.353	.941	.359	.924	.364	.891	.360	.884
.275	1.176	.399	.988	.405	1.006	.400	.988	.405	.970	.411	.936	.407	.923
.326	1.232	.450	1.035	.457	1.054	.451	1.035	.455	1.016	.462	.980	.457	.973
		.505	1.082	.512	1.102	.504	1.082	.507	1.062	.515	1.025	.510	1.017
		.563	1.129	.570	1.150	.560	1.130	.563	1.108	.572	1.069	.566	1.061
		.624	1.177	.632	1.197	.620	1.177	.622	1.155	.633	1.114	.626	1.105
		.689	1.224	.698	1.245	.683	1.224	.684	1.201	.698	1.158	.690	1.149
								.749	1.247	.767	1.203	.757	1.194
										.839	1.247	.829	1.238

TABLE I.- Continued

(d) Values based on reference 14 (Sutton)

Predicted shock shapes for –									
Helium (real)		Air (real)		CF_4 (real)		C_2F_6 (real)		CO_2 (real)	
x/r_n	y/r_n	x/r_n	y/r_n	x/r_n	y/r_n	x/r_n	y/r_n	x/r_n	y/r_n
-0.217	0	-0.072	0	-0.067	0	-0.054	0	-0.043	0
-.212	.122	-.067	.107	-.062	.107	-.049	.105	-.038	.104
-.197	.243	-.053	.213	-.048	.212	-.035	.210	-.023	.207
-.173	.363	-.029	.318	-.024	.317	-.011	.313	.001	.309
-.139	.482	.004	.421	.009	.419	.021	.414	.035	.408
-.095	.598	.045	.522	.050	.519	.063	.512	.077	.504
-.043	.713	.095	.619	.100	.616	.113	.607	.128	.597
.019	.827	.153	.713	.158	.709	.170	.699	.187	.685
.089	.938	.219	.804	.223	.800	.235	.788	.253	.770
.169	1.048	.292	.892	.296	.888	.307	.873	.326	.850
.257	1.157	.373	.977	.375	.973	.386	.956	.405	.927
.356	1.265	.461	1.059	.463	1.056	.473	1.036	.491	1.000
		.557	1.139					.583	1.072
		.662	1.219					.683	1.141

Predicted shock shapes for –									
Helium (ideal)		Air (ideal)		CF_4 (ideal)		C_2F_6 (ideal)		CO_2 (ideal)	
x/r_n	y/r_n	x/r_n	y/r_n	x/r_n	y/r_n	x/r_n	y/r_n	x/r_n	y/r_n
-0.217	0	-0.071	0	-0.065	0	-0.053	0	-0.043	0
-.212	.122	-.066	.107	-.060	.106	-.049	.105	-.038	.104
-.1975	.243	-.051	.213	-.046	.212	-.034	.210	-.023	.207
-.173	.363	-.027	.318	-.022	.316	-.011	.313	.001	.309
-.139	.482	.006	.420	.011	.418	.022	.413	.034	.408
-.095	.598	.048	.520	.053	.518	.064	.511	.076	.505
-.043	.713	.099	.617	.103	.614	.114	.606	.127	.597
.019	.827	.158	.710	.161	.707	.171	.698	.186	.686
.089	.938	.224	.799	.227	.796	.237	.786	.252	.771
.169	1.048	.297	.886	.299	.883	.309	.871	.324	.851
.257	1.157	.378	.969	.379	.967	.388	.953	.404	.928
.356	1.265	.466	1.050	.467	1.048	.474	1.034	.490	1.002
		.561	1.128	.561	1.128	.568	1.112	.583	1.074
		.665	1.206	.665	1.207	.670	1.190	.683	1.143

TABLE I.- Concluded

(e) Values based on reference 16 (Grose)

Predicted shock shapes for – Nonequilibrium CO_2	
x/r_n	y/r_n
-0.043	0
-.039	.1
-.026	.2
-.004	.3
.027	.4
.068	.5
.120	.6
.184	.7
.262	.8
.357	.9
.474	1.0
.616	1.1
.790	1.2

(f) Values based on reference 19 (Moss)

Predicted shock shapes for – Nonequilibrium air	
x/r_n	y/r_n
-0.080	0
-.076	.108
-.062	.215
-.040	.322
-.008	.426
.033	.528
.082	.628
.139	.726
.199	.825

(g) Values based on reference 18 (Anderson and Moss)

Predicted shock shapes for –					
Helium (ideal)			Air (real)		
x/r_n	y/r_n	δ^*/r_n	x/r_n	y/r_n	δ^*/r_n
-0.225	0	-----	-0.071	0	-----
-.206	.244	3.448^{-3}	-.055	.214	7.113^{-4}
-.136	.494	3.551^{-3}	.003	.422	7.500^{-4}
-.020	.745	3.889^{-3}	.094	.620	8.461^{-4}
.140	.969	5.487^{-3}	.226	.794	1.105^{-3}

(h) Values based on Hamilton's method

Predicted shock shapes for –									
Helium (ideal)		Air (ideal)		CF_4 (ideal)		C_2F_6 (ideal)		CO_2 (ideal)	
x/r_n	y/r_n	x/r_n	y/r_n	x/r_n	y/r_n	x/r_n	y/r_n	x/r_n	y/r_n
-0.217	0	-0.071	0	-0.065	0	-0.053	0	-0.043	0
-.208	.164	-.064	.128	-.058	.127	-.046	.124	-.036	.122
-.181	.326	-.043	.255	-.038	.252	-.026	.246	-.016	.242
-.136	.486	-.008	.379	-.004	.375	.007	.367	.017	.360
-.075	.642	.039	.500	.042	.495	.052	.483	.062	.474
.003	.796	.099	.616	.101	.610	.108	.596	.119	.584
.097	.945	.170	.727	.170	.720	.176	.704	.187	.688

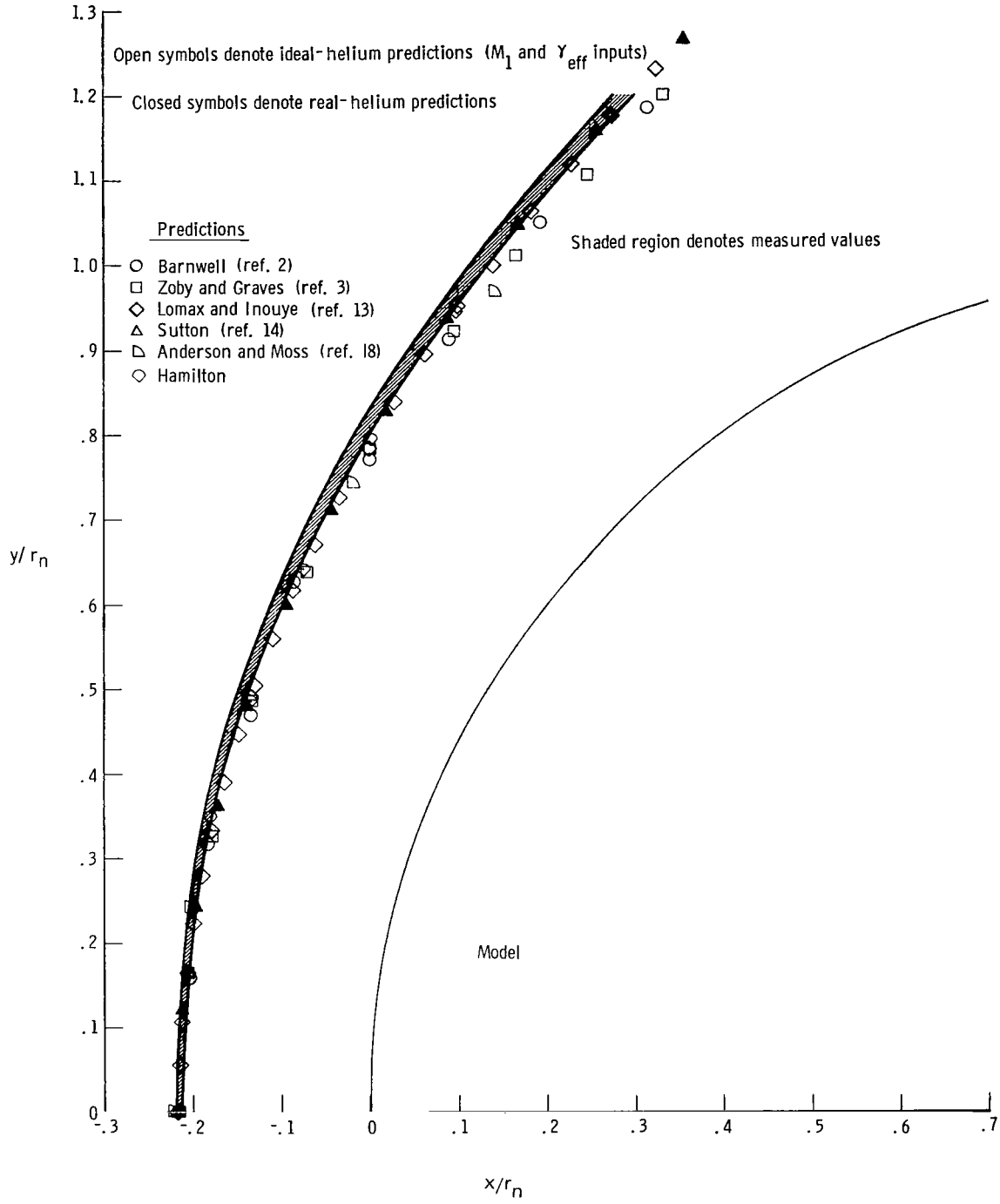

(a) Helium. $M_1 = 6.02$; $\epsilon = 3.69$.

Figure 1.- Measured and predicted shock shapes for sphere in perfect helium, near perfect CF_4 and C_2F_6 test gases.

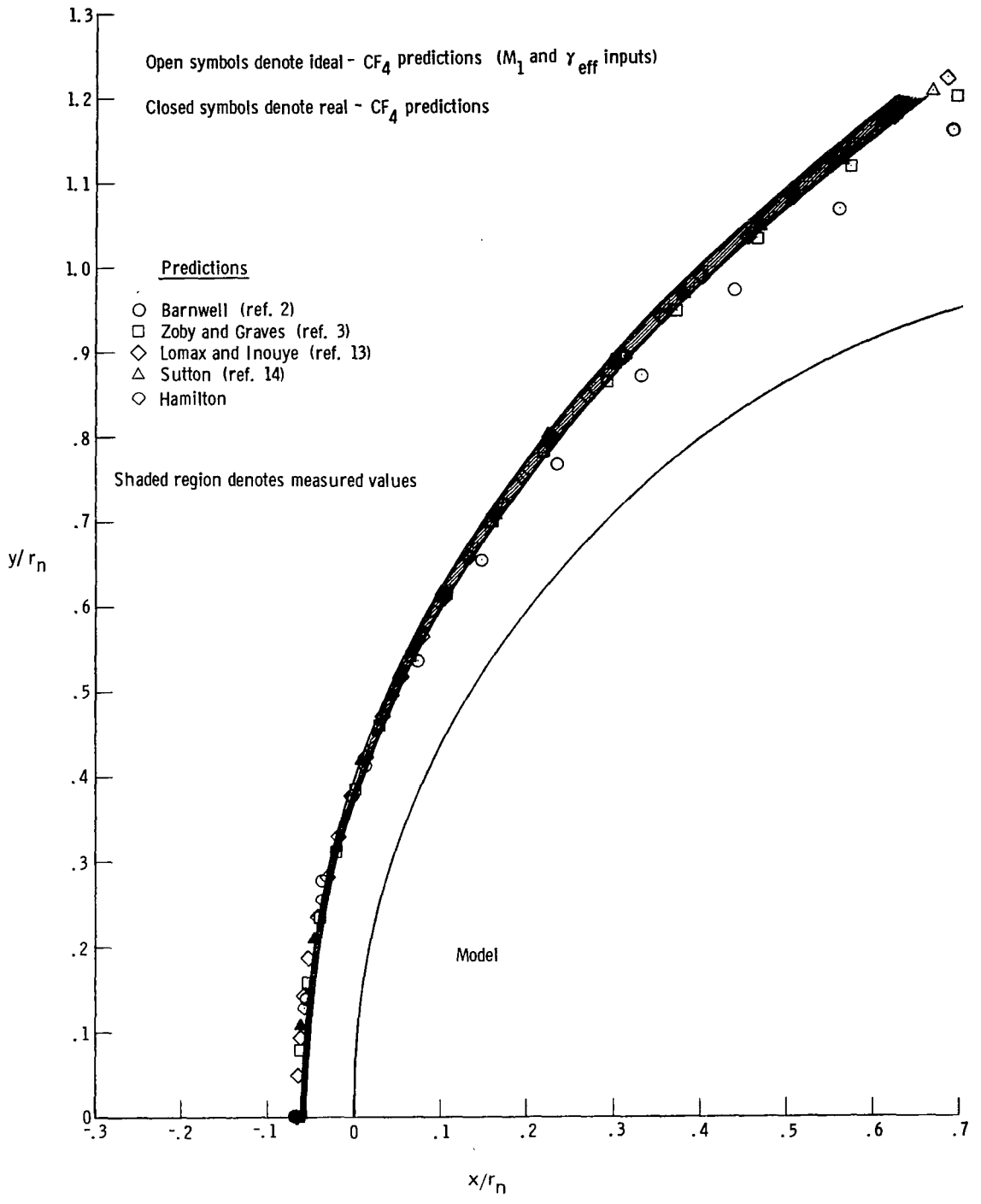

(b) CF_4. $M_1 = 6.15$; $\epsilon = 12.2$.

Figure 1.- Continued.

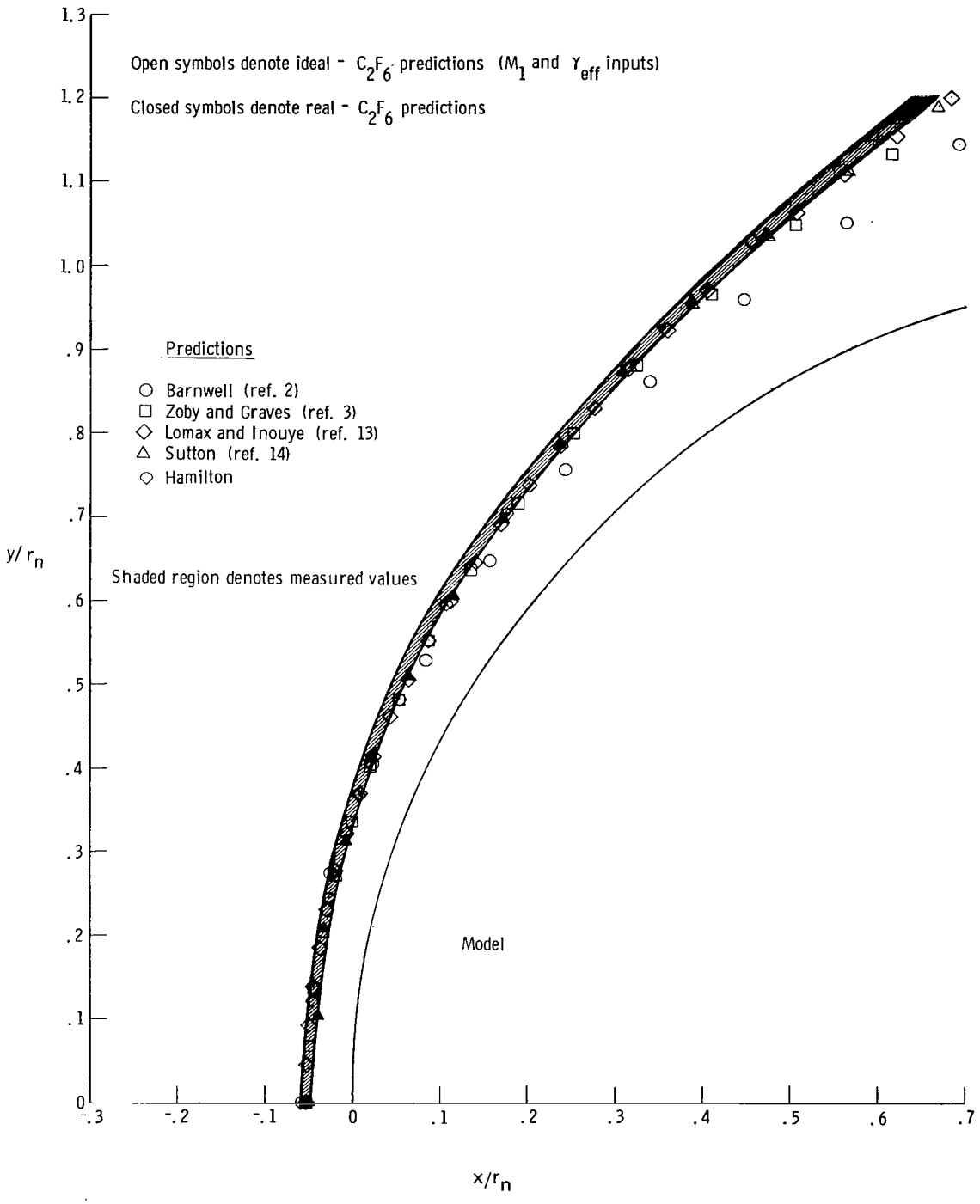

(c) C_2F_6. $M_1 = 5.35$; $\epsilon = 15.1$.

Figure 1.- Concluded.

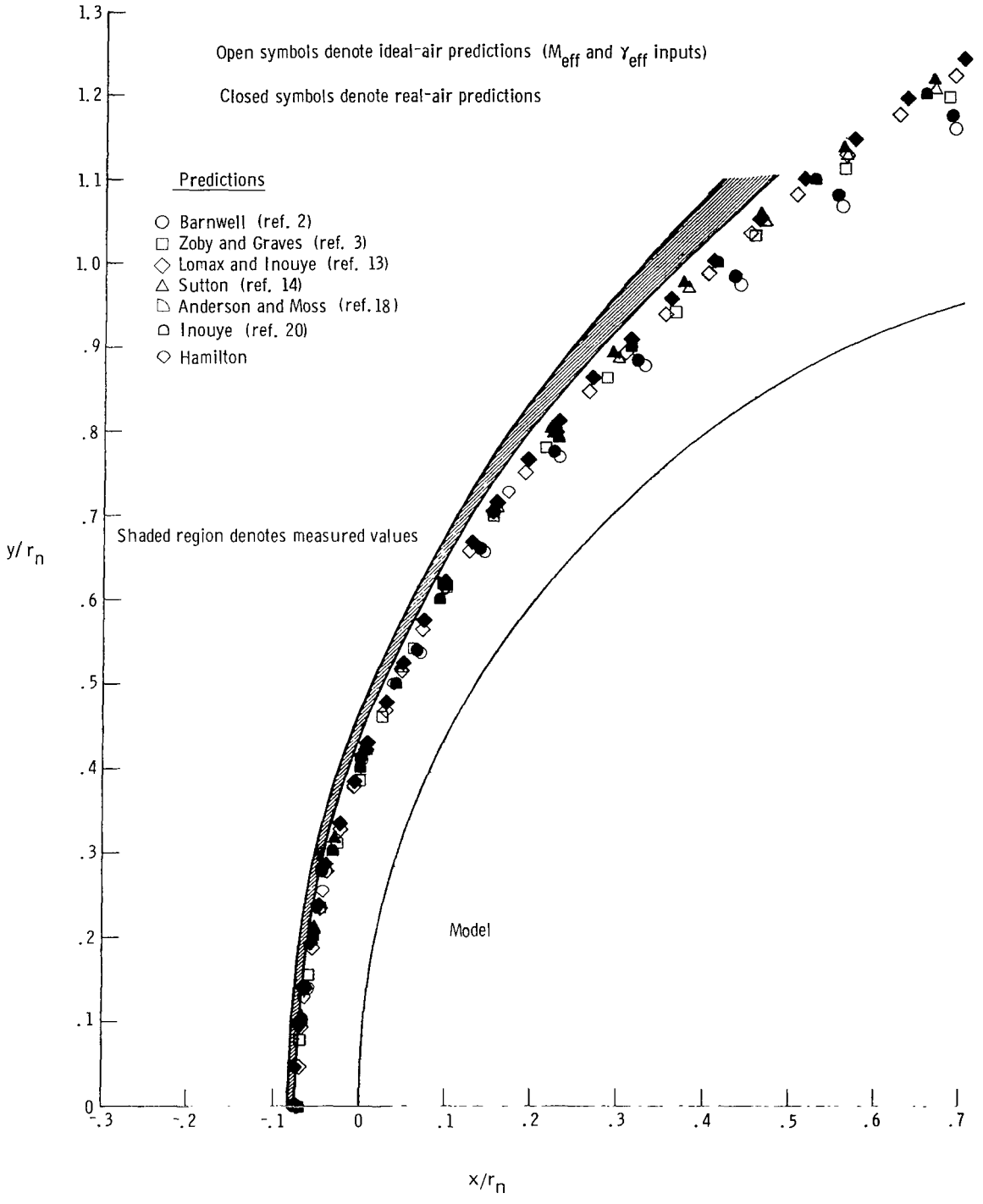

(a) Air. $M_1 = 7.72$; $\epsilon = 11.11$.

Figure 2.- Measured and predicted shock shapes for sphere in real air and CO_2 test gases.

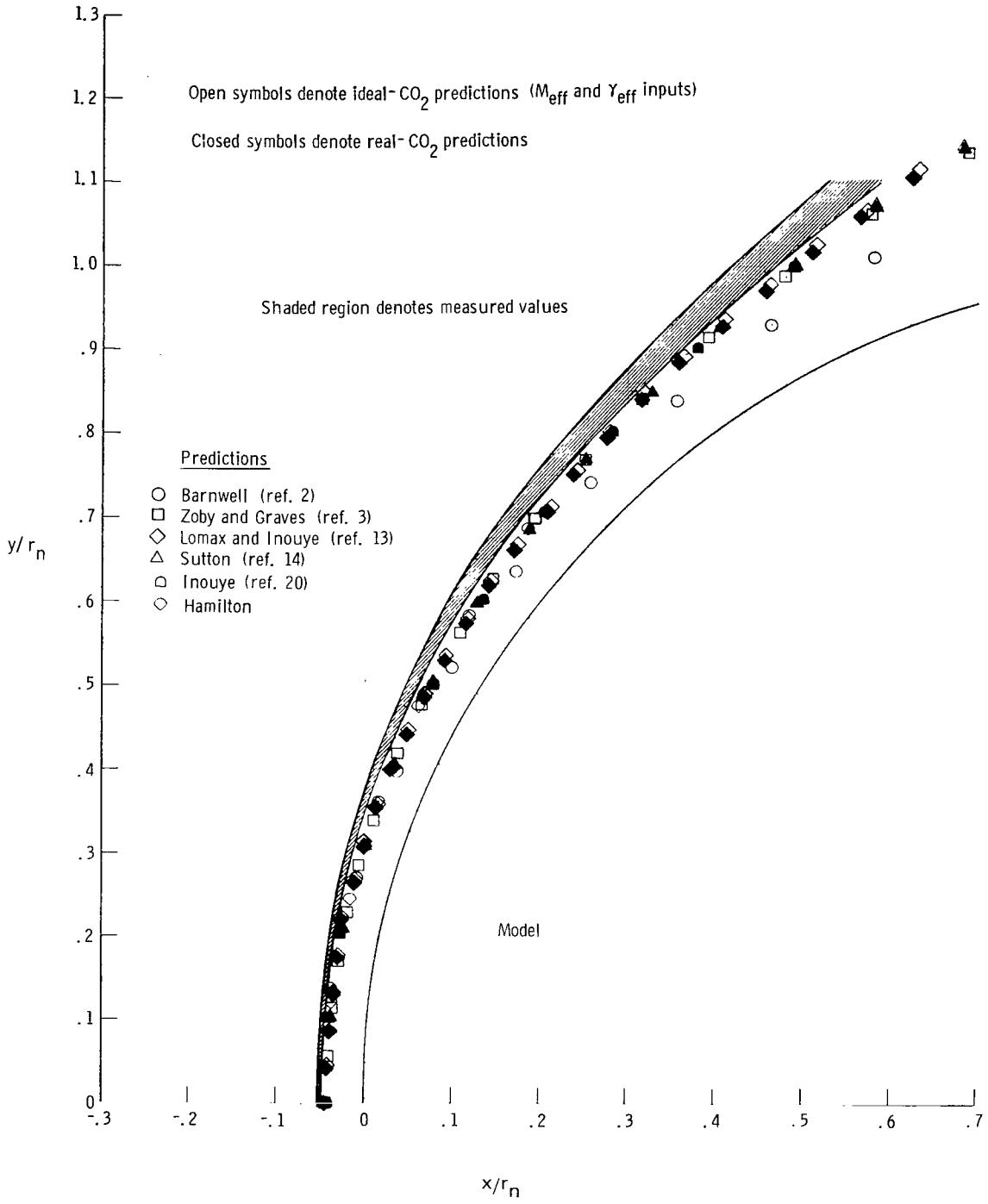

(b) CO_2. $M_1 = 9.18$; $\epsilon = 18.81$.

Figure 2.- Concluded.

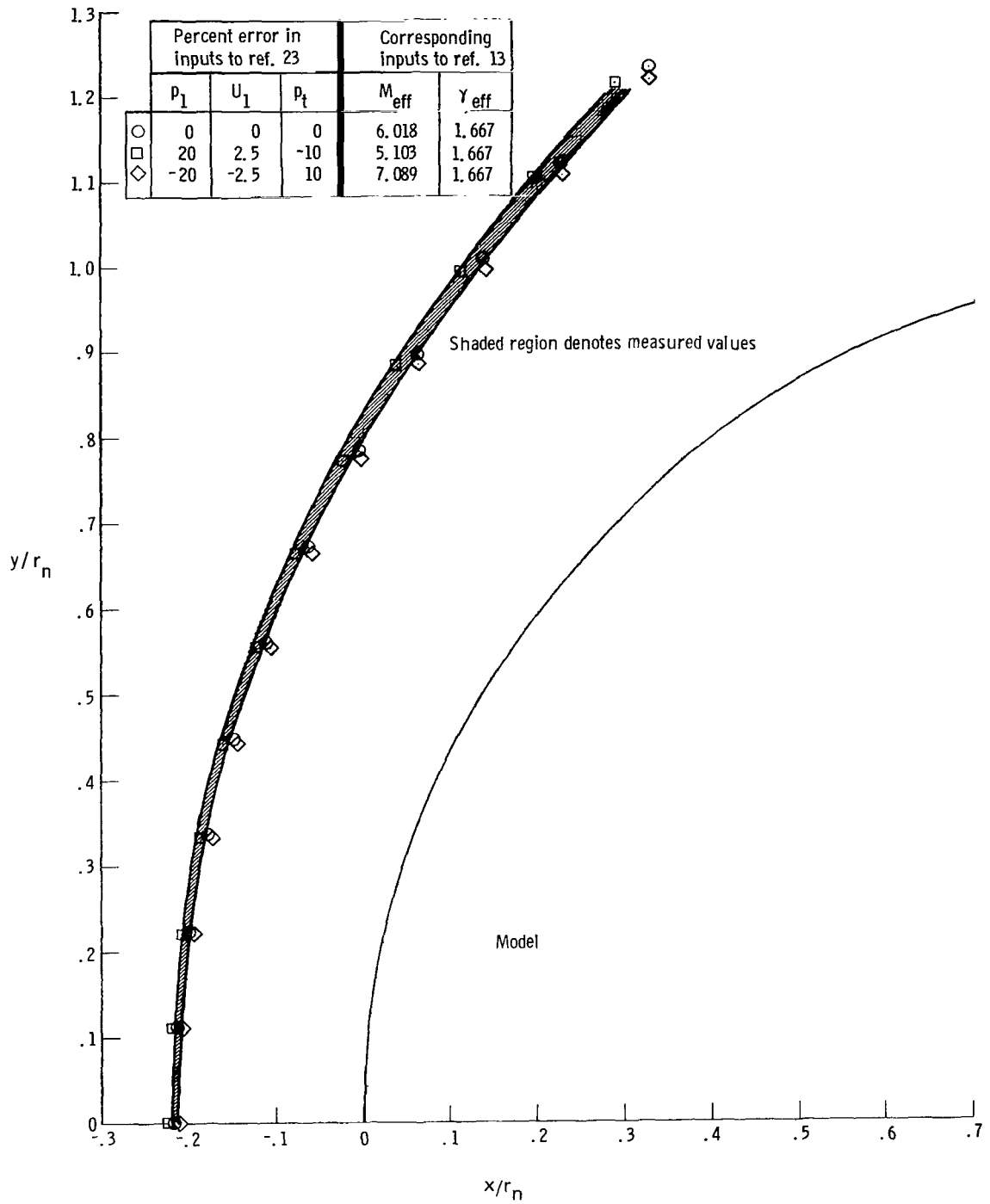

(a) Helium.

Figure 3.- Effect of uncertainties in inputs to program of reference 23 on predicted shock shape for a sphere.

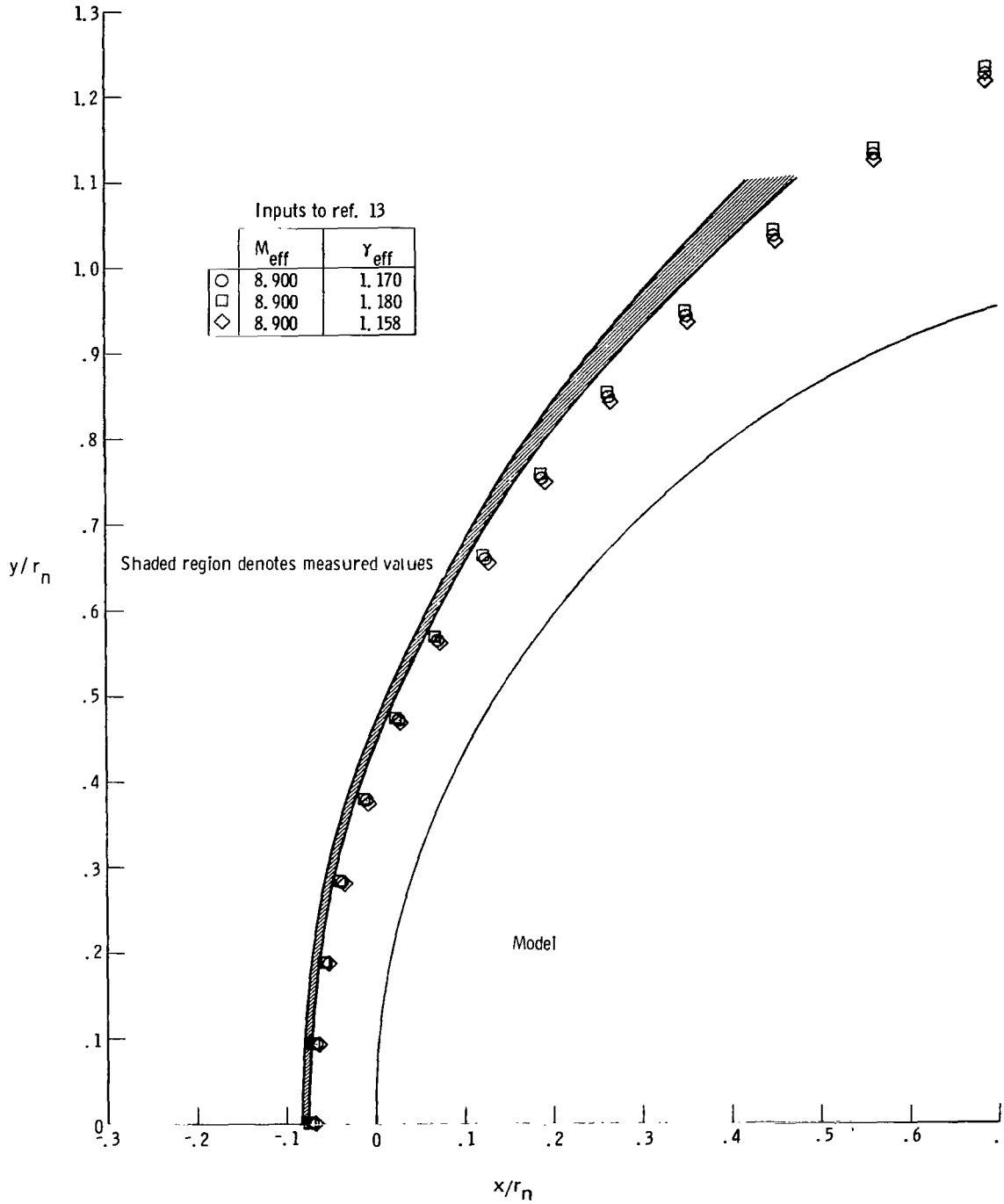

(b) Air.

Figure 3.- Continued.

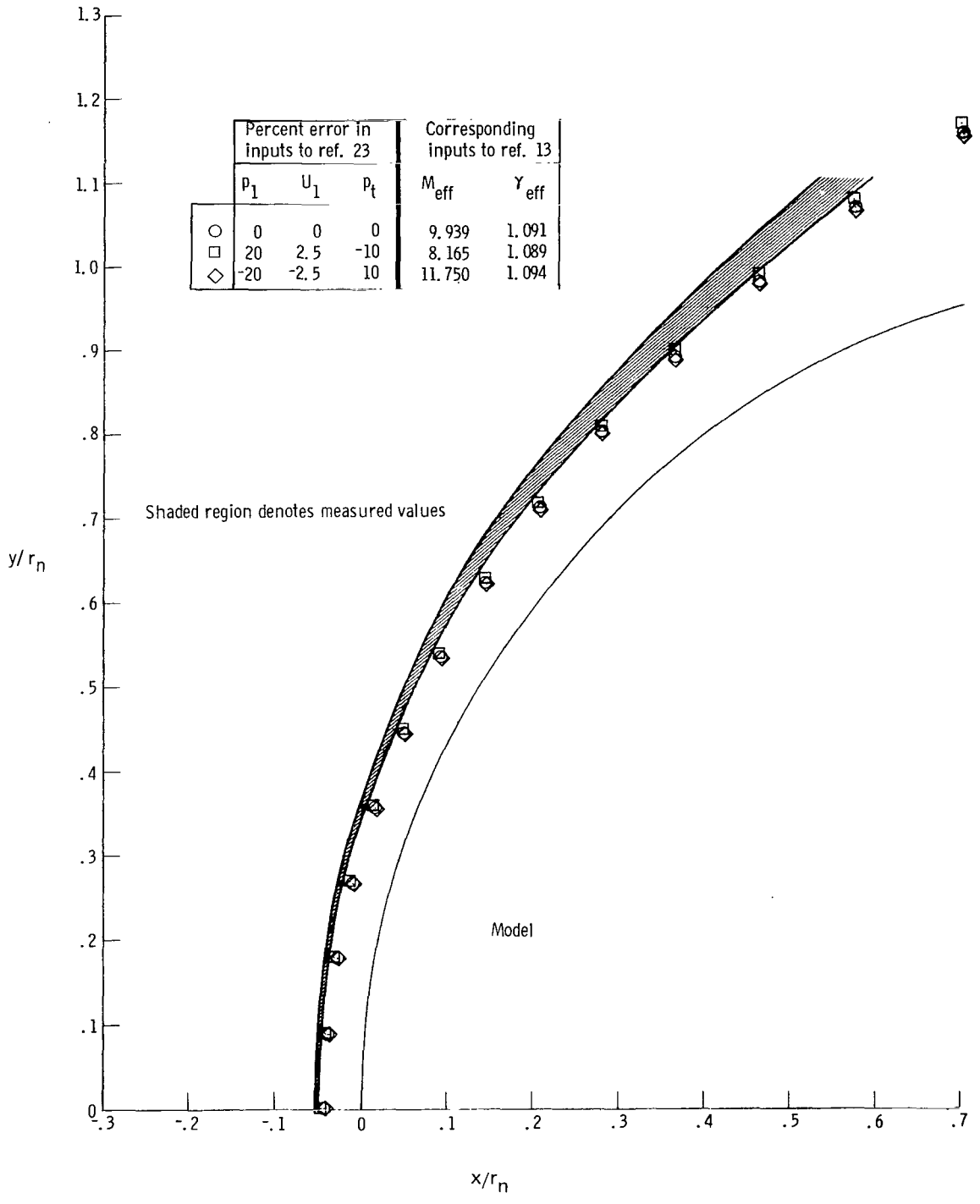

(c) CO_2.

Figure 3.- Concluded.

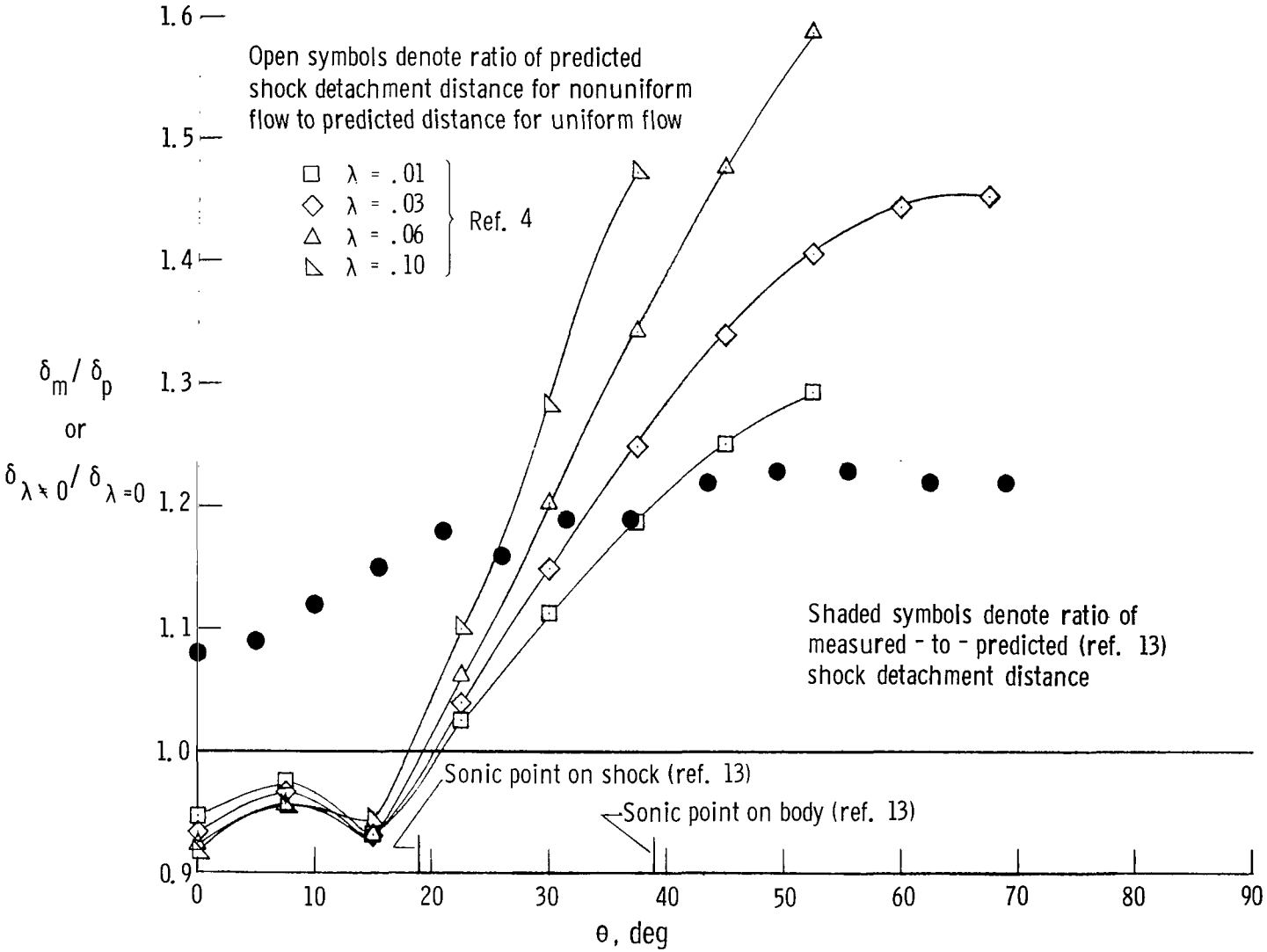

Figure 4.- Comparison of measured shock detachment distance on a sphere to that predicted for nonuniform free-stream flow in air.

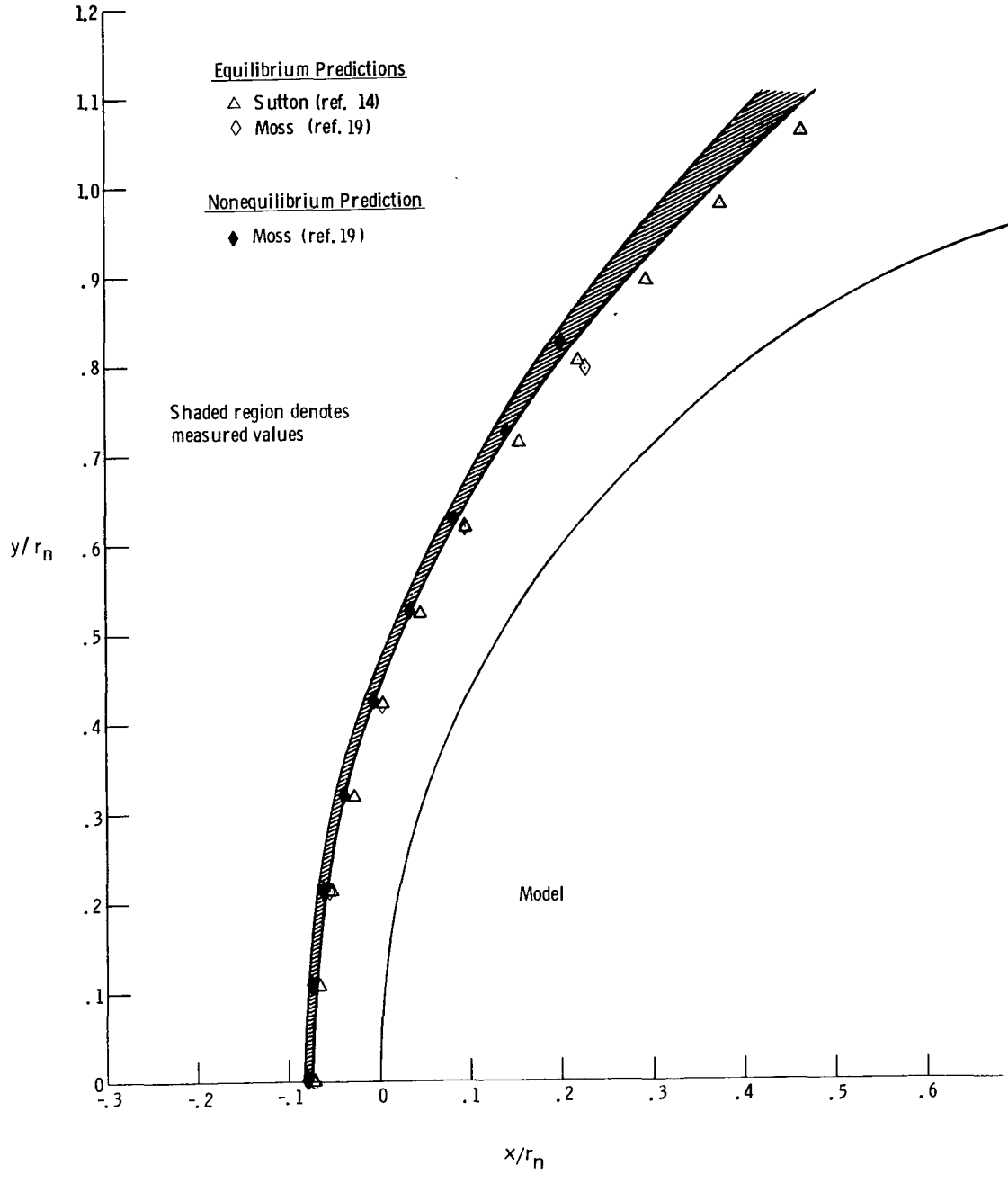

(a) Air.

Figure 5.- Effect of nonequilibrium flow within the shock layer on predicted shock shape for a 3.18-cm-radius sphere.

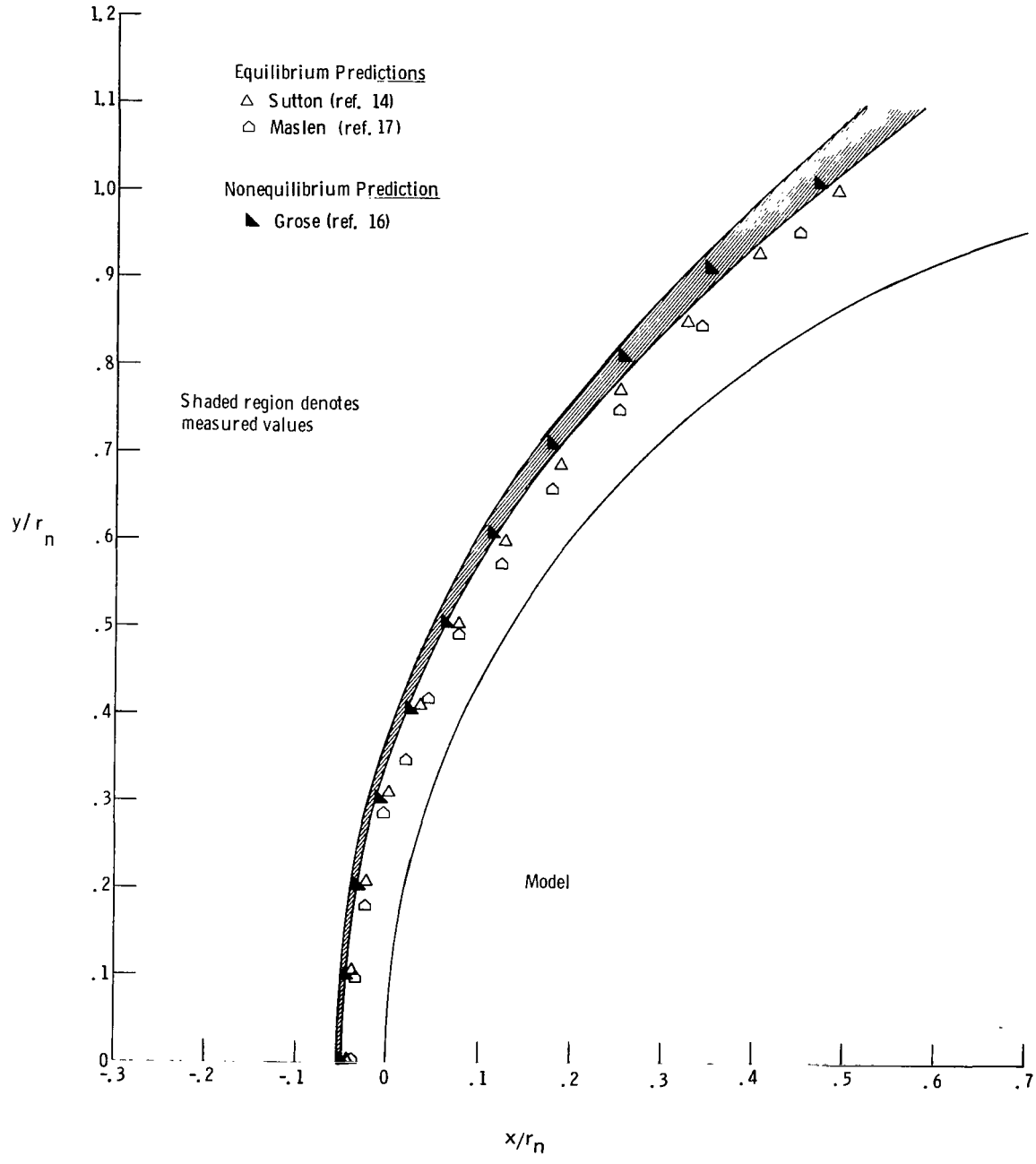

(b) CO_2.

Figure 5.- Concluded.

NATIONAL AERONAUTICS AND SPACE ADMINISTRATION
WASHINGTON, D.C. 20546

OFFICIAL BUSINESS
PENALTY FOR PRIVATE USE $300

SPECIAL FOURTH-CLASS RATE BOOK

POSTAGE AND FEES PAID
NATIONAL AERONAUTICS AND SPACE ADMINISTRATION
451

U.S.MAIL

"The aeronautical and space activities of the United States shall be conducted so as to contribute . . . to the expansion of human knowledge of phenomena in the atmosphere and space. The Administration shall provide for the widest practicable and appropriate dissemination of information concerning its activities and the results thereof."

—NATIONAL AERONAUTICS AND SPACE ACT OF 1958

NASA SCIENTIFIC AND TECHNICAL PUBLICATIONS

TECHNICAL REPORTS: Scientific and technical information considered important, complete, and a lasting contribution to existing knowledge.

TECHNICAL NOTES: Information less broad in scope but nevertheless of importance as a contribution to existing knowledge.

TECHNICAL MEMORANDUMS: Information receiving limited distribution because of preliminary data, security classification, or other reasons. Also includes conference proceedings with either limited or unlimited distribution.

CONTRACTOR REPORTS: Scientific and technical information generated under a NASA contract or grant and considered an important contribution to existing knowledge.

TECHNICAL TRANSLATIONS: Information published in a foreign language considered to merit NASA distribution in English.

SPECIAL PUBLICATIONS: Information derived from or of value to NASA activities. Publications include final reports of major projects, monographs, data compilations, handbooks, sourcebooks, and special bibliographies.

TECHNOLOGY UTILIZATION PUBLICATIONS: Information on technology used by NASA that may be of particular interest in commercial and other non-aerospace applications. Publications include Tech Briefs, Technology Utilization Reports and Technology Surveys.

Details on the availability of these publications may be obtained from:

SCIENTIFIC AND TECHNICAL INFORMATION OFFICE

NATIONAL AERONAUTICS AND SPACE ADMINISTRATION

Washington, D.C. 20546